Contents for Annexure

Annexure 1

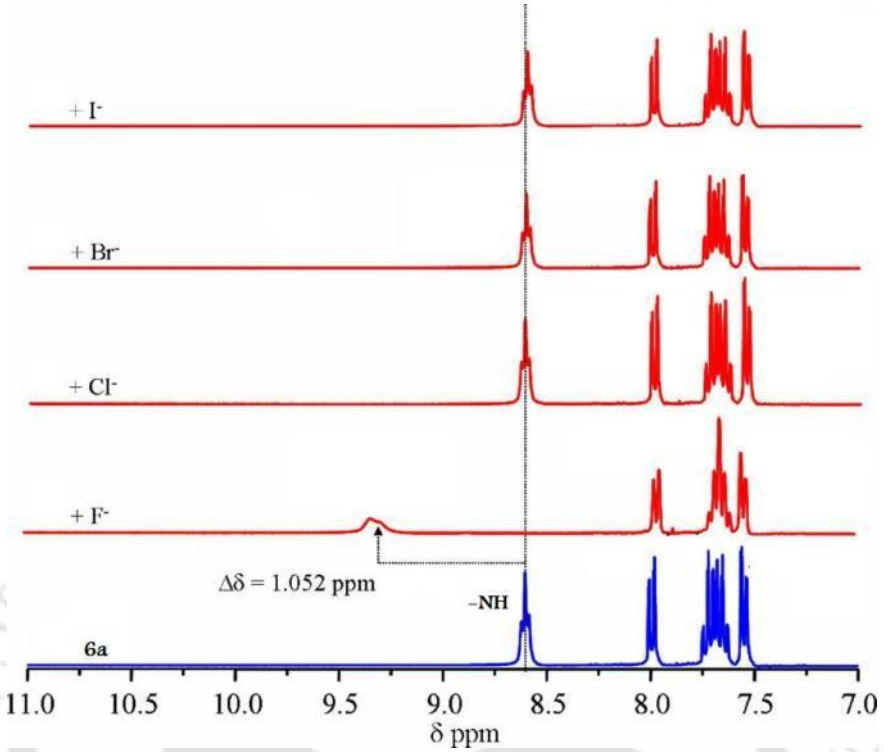

Figure A1.1 Partial ^{1}H NMR (300 MHz) spectra of receptor **6a** in DMSO-d_6 with (TBA)X^- (where X^- = F^-, Cl^-, Br^- and I^-) at 298 K.

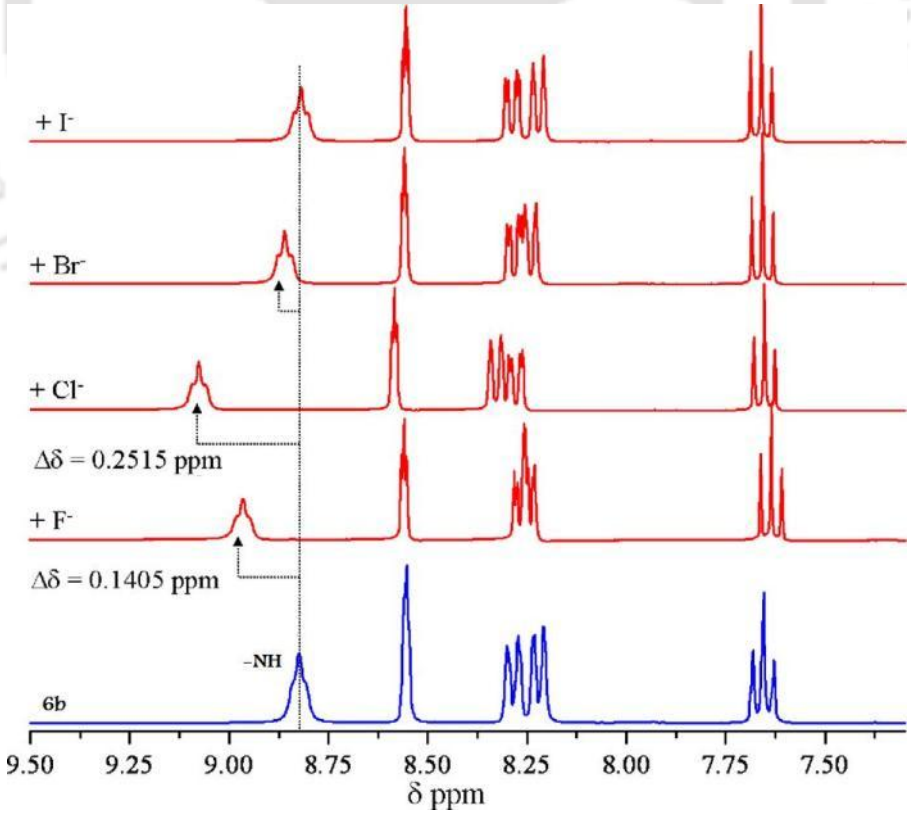

Figure A1.2 Partial ^{1}H NMR (300 MHz) spectra of receptor **6b** in DMSO-d_6 with (TBA)X^- (where X^- = F^-, Cl^-, Br^- and I^-) at 298 K.

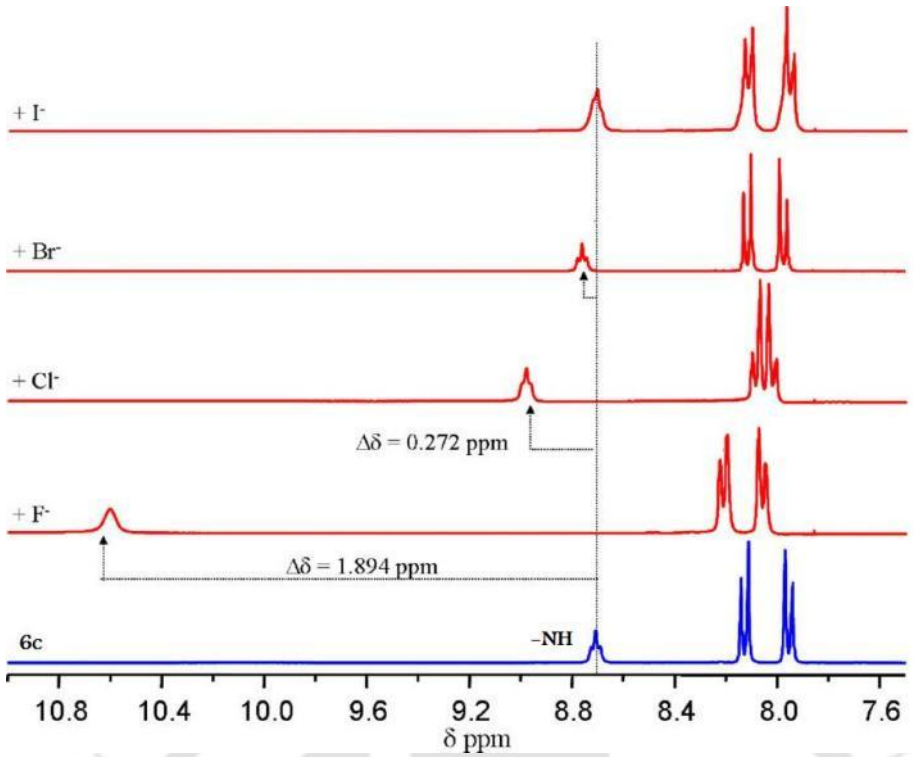

Figure A1.3 Partial ^{1}H NMR (300 MHz) spectra of receptor **6c** in DMSO-d_6 with (TBA)X^- (where X^- = F^-, Cl^-, Br^- and I^-) at 298 K.

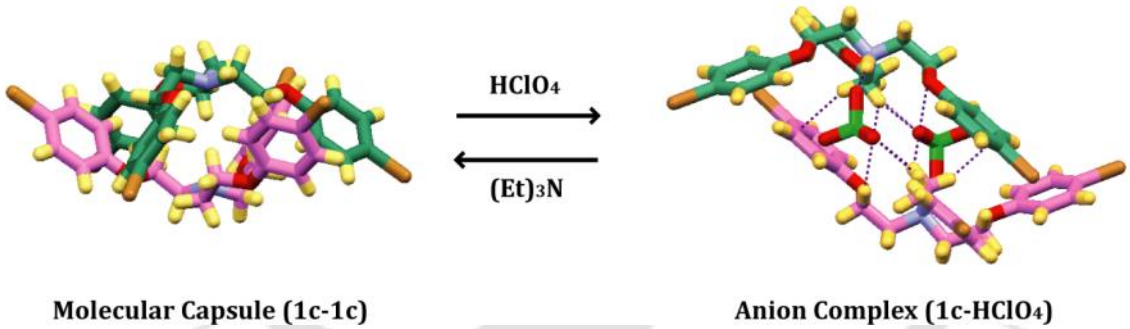

Figure A1.4 pH-modulated reversible exchange between molecular capsule (**1c•1c**) and its anion (ClO_4^-) complex.

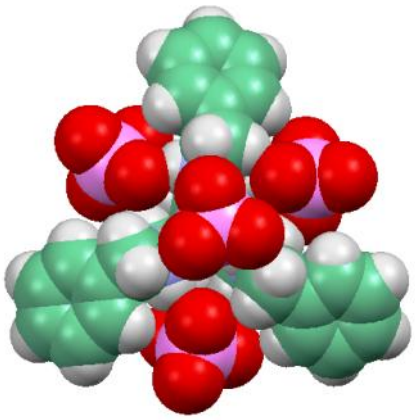

Figure A1.5 Spacefill model of the crystal structure of [(H_3**2a**)($H_2PO_4^-$)$_3$]•H_3PO_4 showing the binding of three $H_2PO_4^-$ counter anions between each receptor side arms and an additional H_3PO_4 molecule above the quasi-planar tripod.

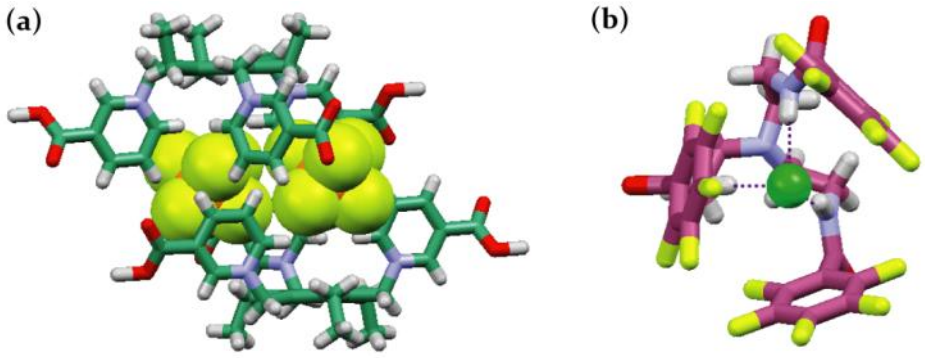

Figure A1.6 (a) Non-capsular aggregation of complex [H**3a**·PF_6·$2H_2O$], and (b) encapsulation of a naked Cl^- anion by receptor **6d**.

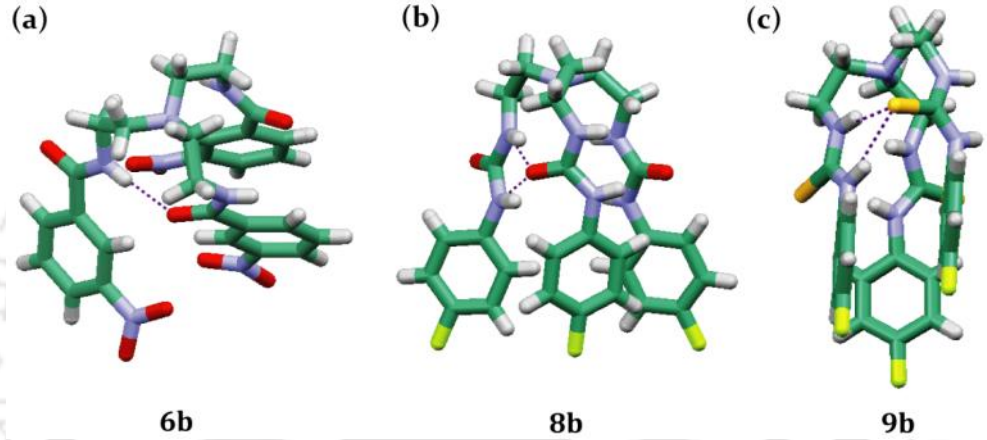

Figure A1.7 Intramolecular N-H···X=C (X = O/S) hydrogen bonding interactions between the receptor side arms of amide **6b**, urea **8b** and thiourea **9b**.

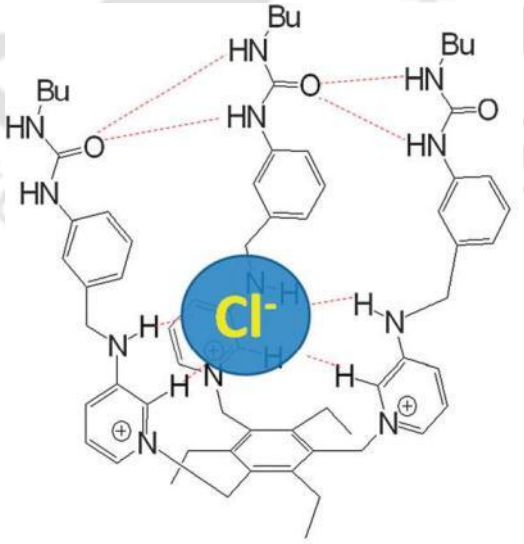

Figure A1.8 Chloride binding assisted formation of unimolecular capsule in receptor **12**.

Annexure 2

Characterization data of receptors, L_1-L_5:

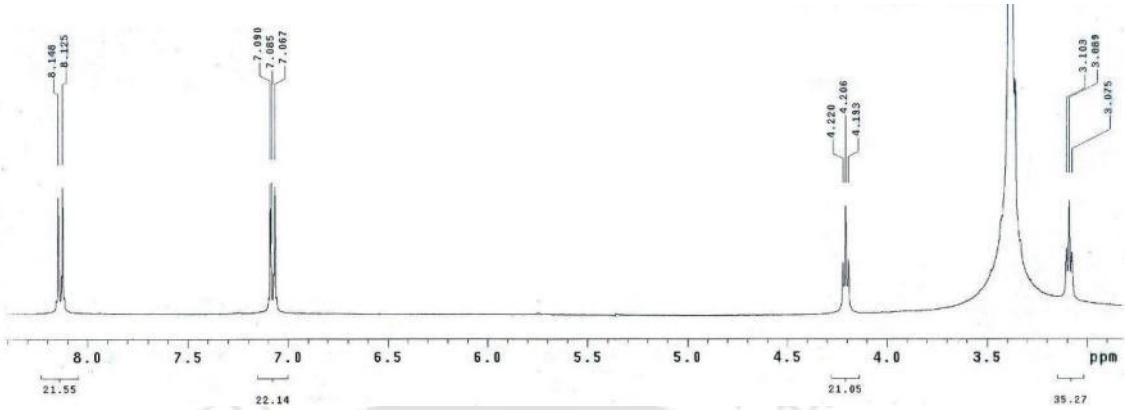

Figure A2.1 ^{1}H NMR spectrum of receptor $\mathbf{L_1}$ (400 MHz, DMSO-d_6).

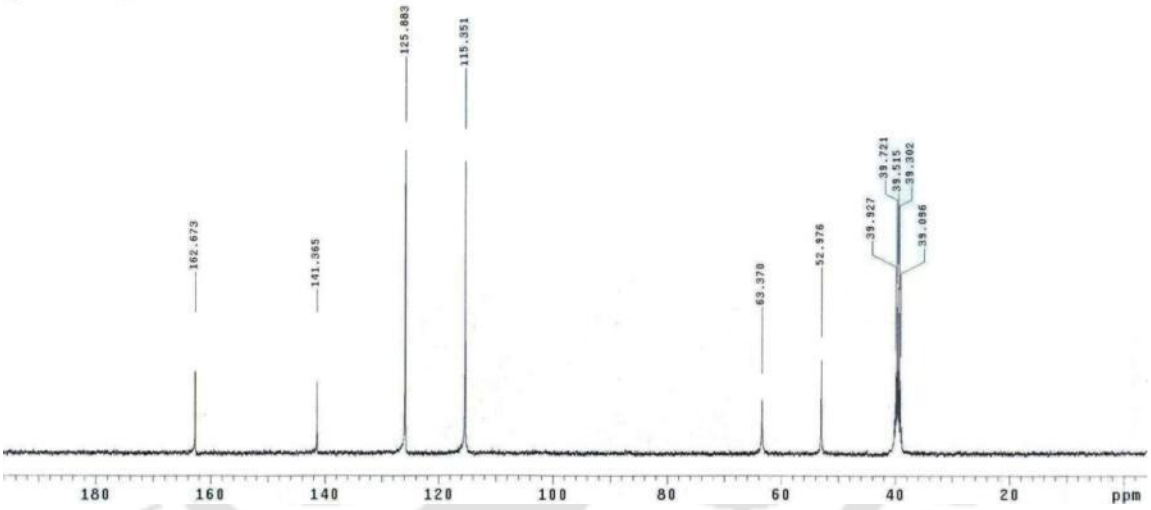

Figure A2.2 ^{13}C NMR spectrum of receptor $\mathbf{L_1}$ (100 MHz, DMSO-d_6).

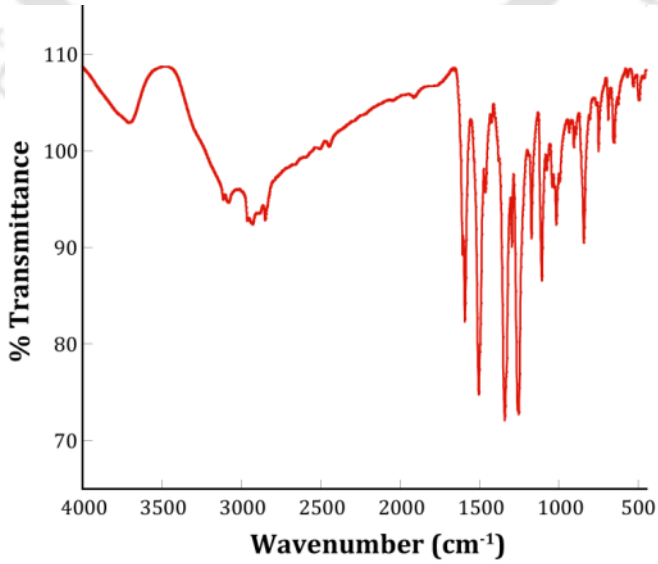

Figure A2.3 FT-IR spectrum of $\mathbf{L_1}$ recorded in KBr pellet.

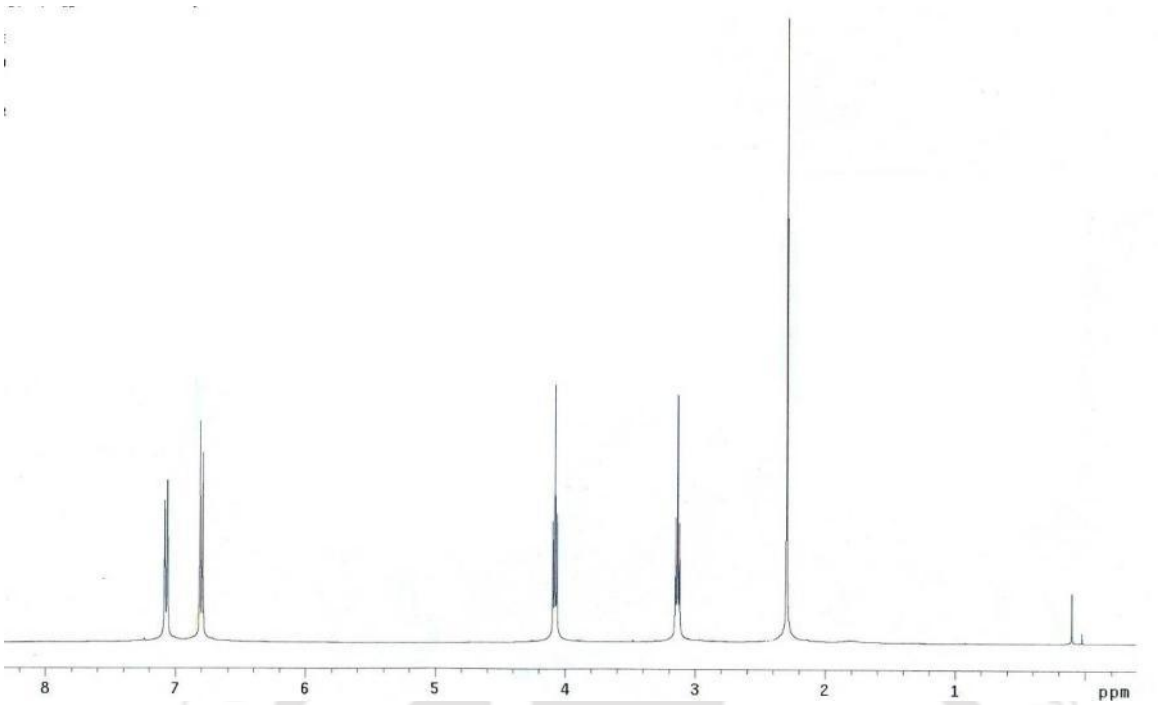

Figure A2.4 ^{1}H NMR spectrum of receptor $\mathbf{L_2}$ (400 MHz, $CDCl_3$).

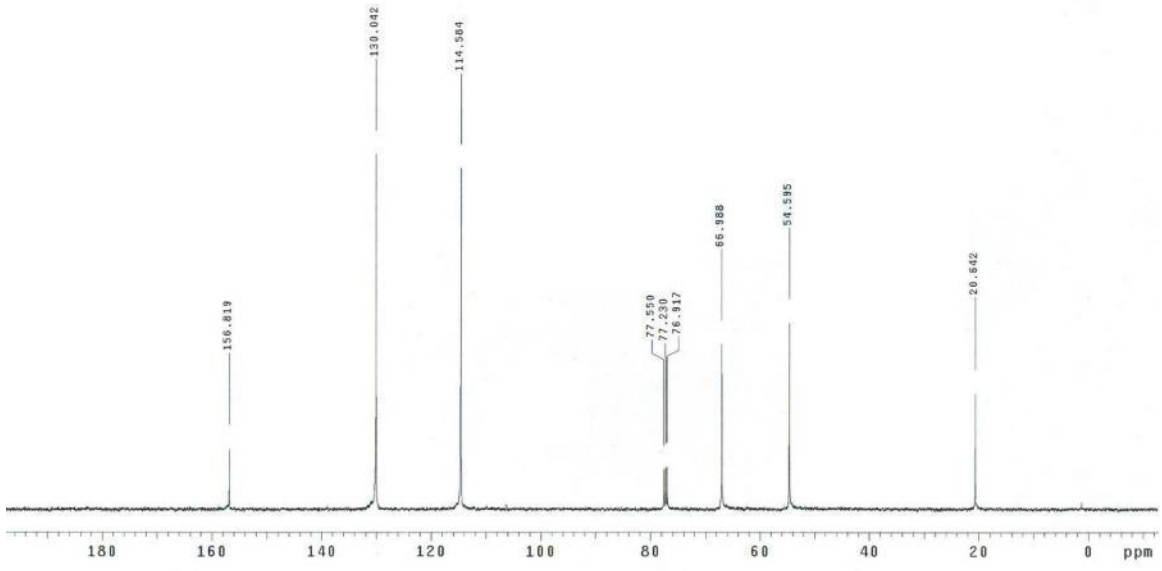

Figure A2.5 ^{13}C NMR spectrum of receptor $\mathbf{L_2}$ (100 MHz, $CDCl_3$).

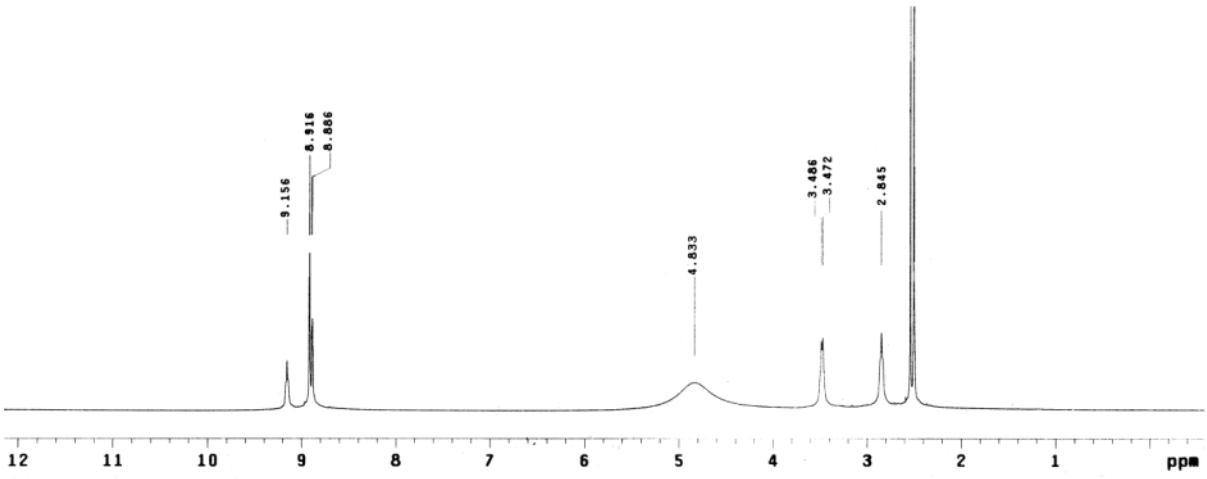

Figure A2.6 ^{1}H NMR spectrum of receptor $\mathbf{L_3}$ (400 MHz, DMSO-d_6).

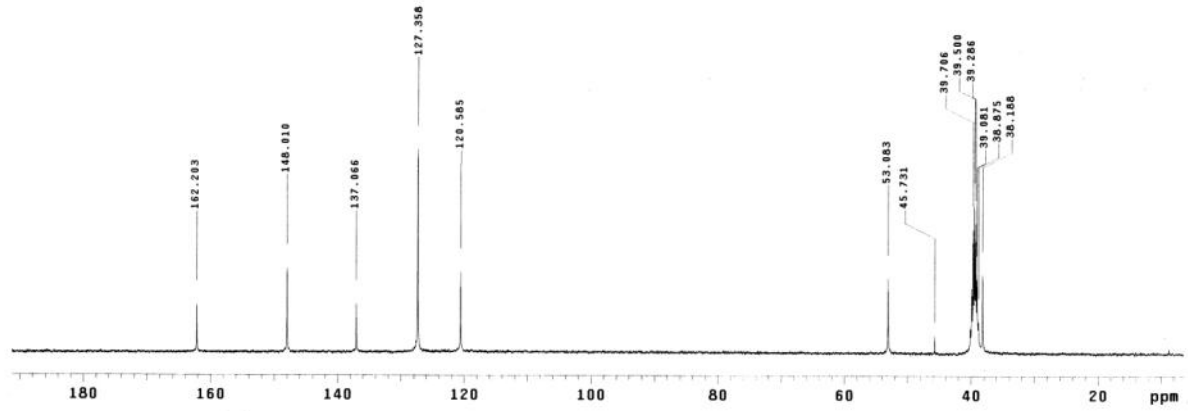

Figure A2.7 ^{13}C NMR spectrum of receptor $\mathbf{L_3}$ (100 MHz, DMSO-d_6).

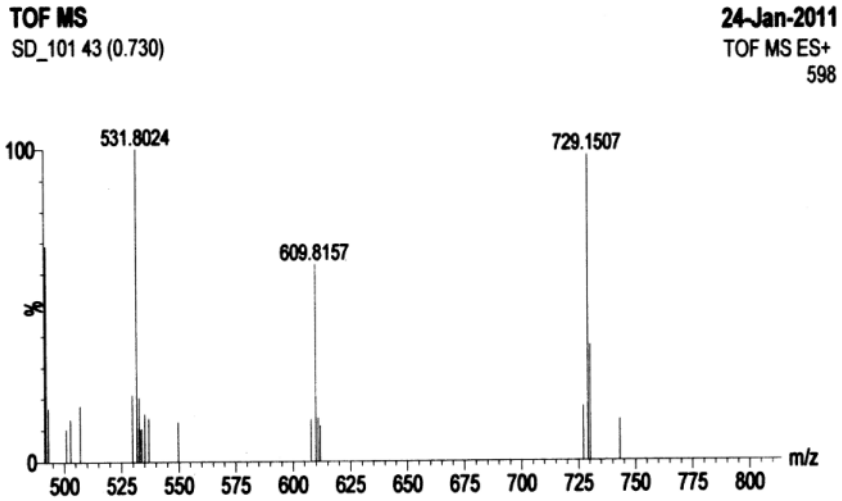

Figure A2.8 ESI-mass spectrum of $\mathbf{L_3}$ showing m/z = 729.150 corresponds to $[M+1]^+$.

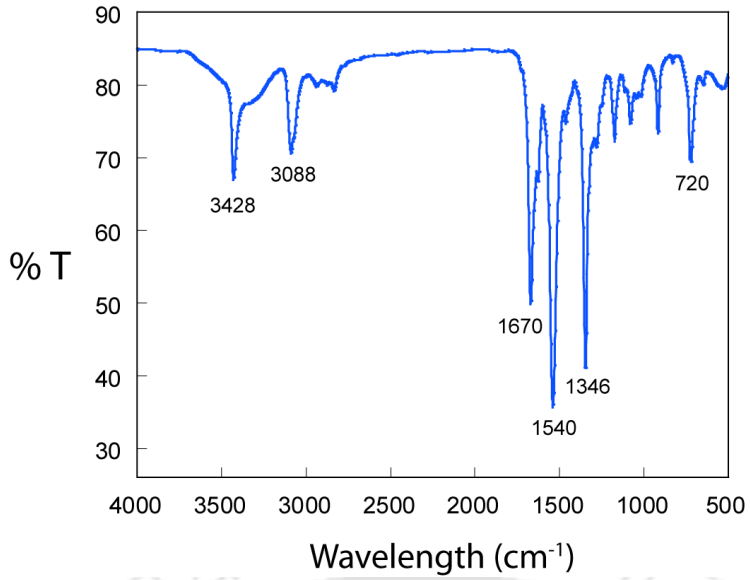

Figure A2.9 FT-IR spectrum of $\mathbf{L_3}$ recorded in KBr pellet.

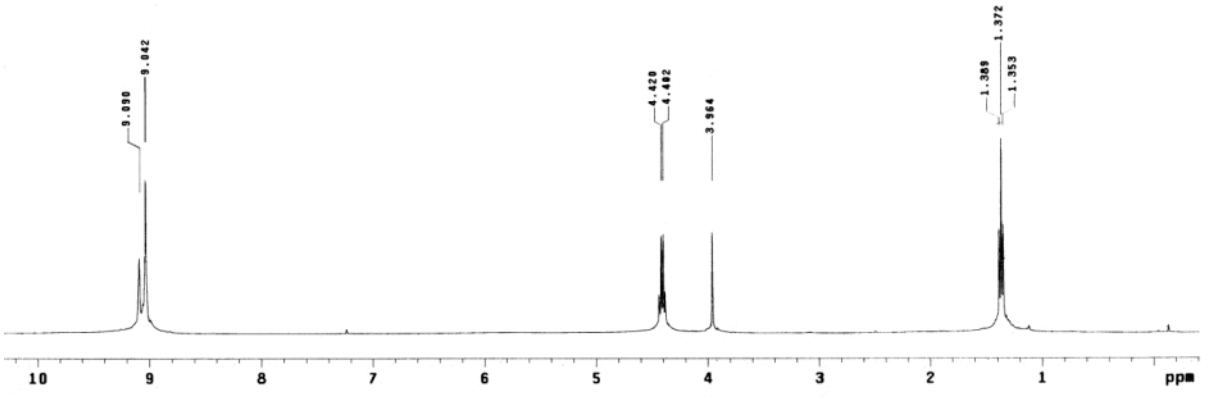

Figure A2.10 ^{1}H NMR spectrum of receptor $\mathbf{CL_3}$ (400 MHz, $CDCl_3$).

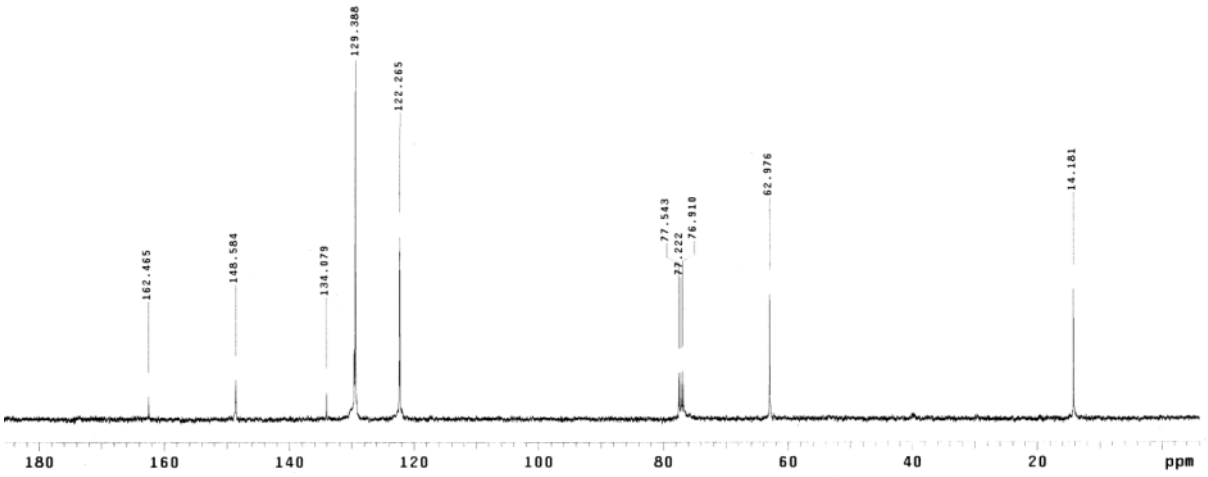

Figure A2.11 ^{13}C NMR spectrum of receptor $\mathbf{CL_3}$ (100 MHz, $CDCl_3$).

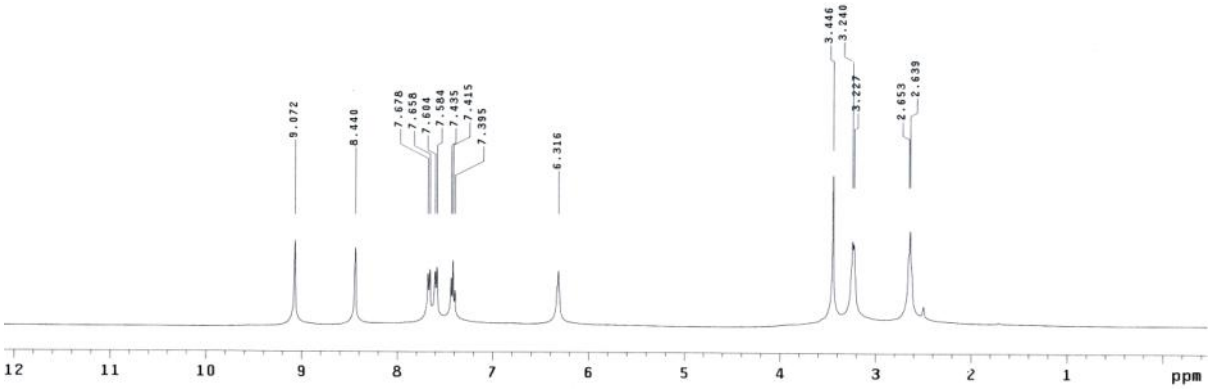

Figure A2.12 [1]H NMR spectrum of receptor **L_4** (400 MHz, DMSO-d_6).

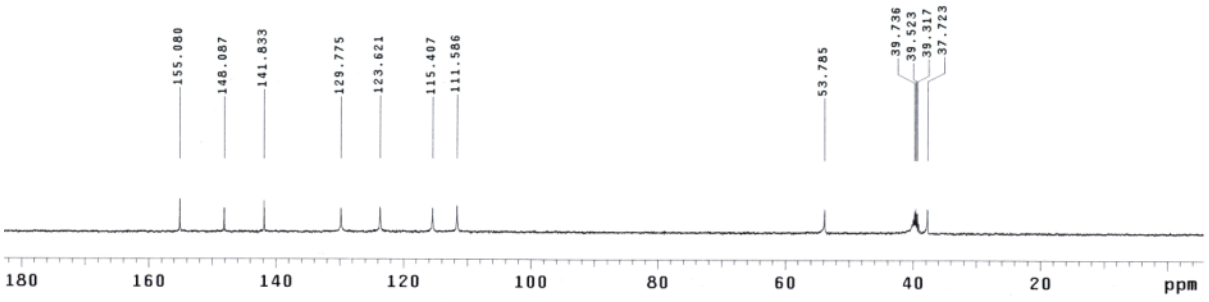

Figure A2.13 [13]C NMR spectrum of receptor **L_4** (100 MHz, DMSO-d_6).

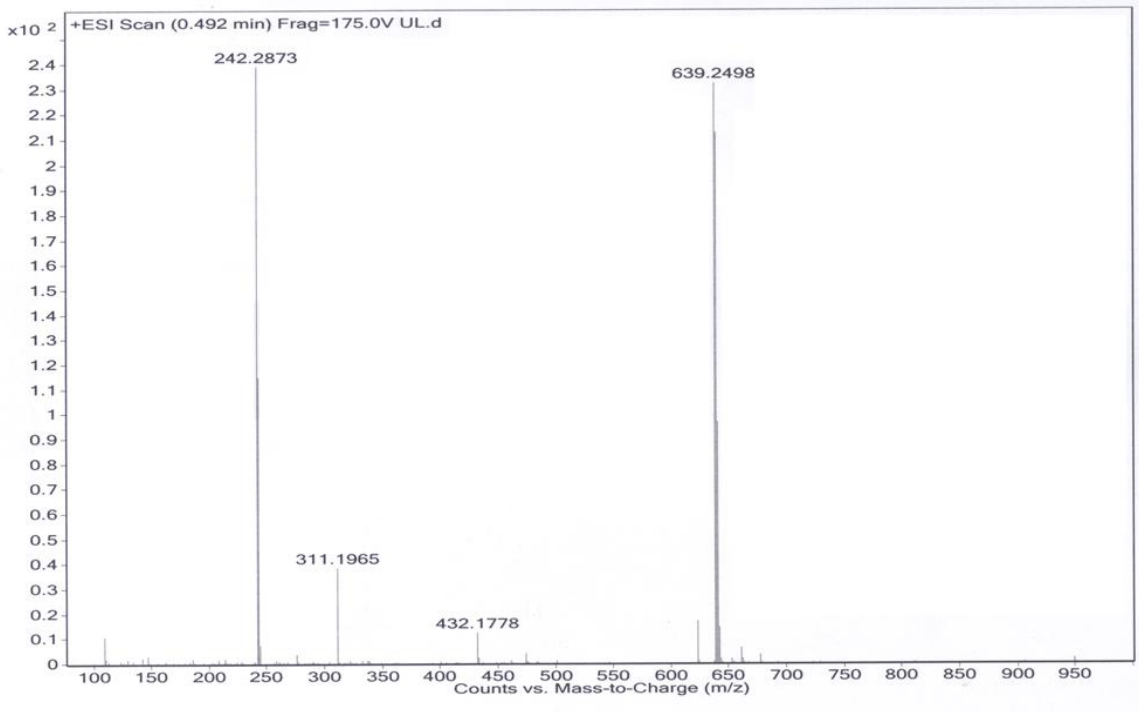

Figure A2.14 ESI-mass spectrum of **L_4** showing m/z = 639.249 corresponds to $[M+1]^+$.

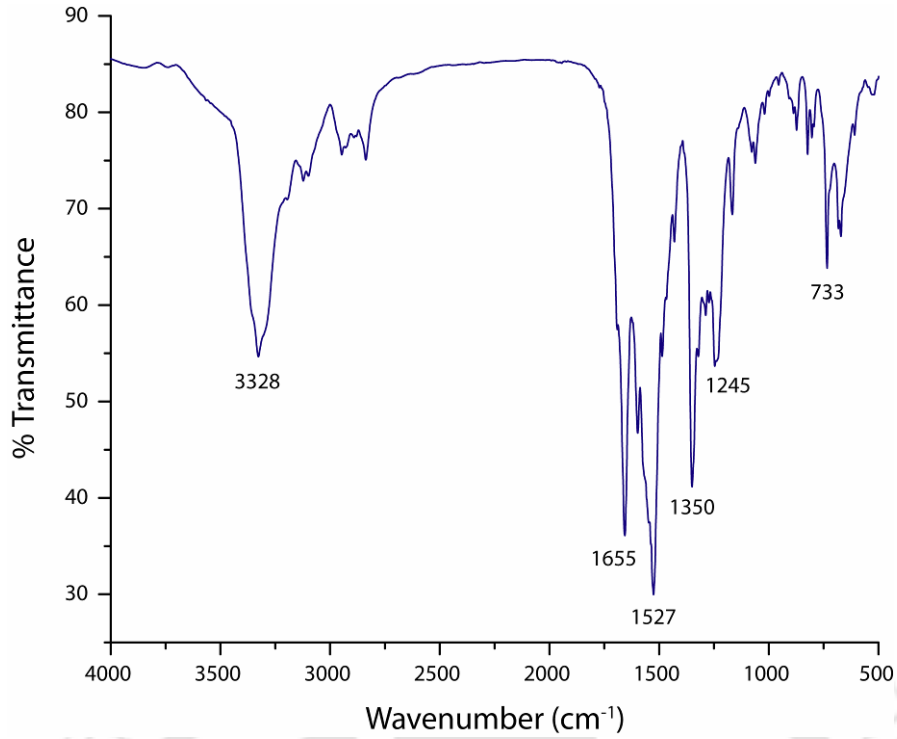

Figure A2.15 FT-IR spectrum of $\mathbf{L_4}$ recorded in KBr pellet.

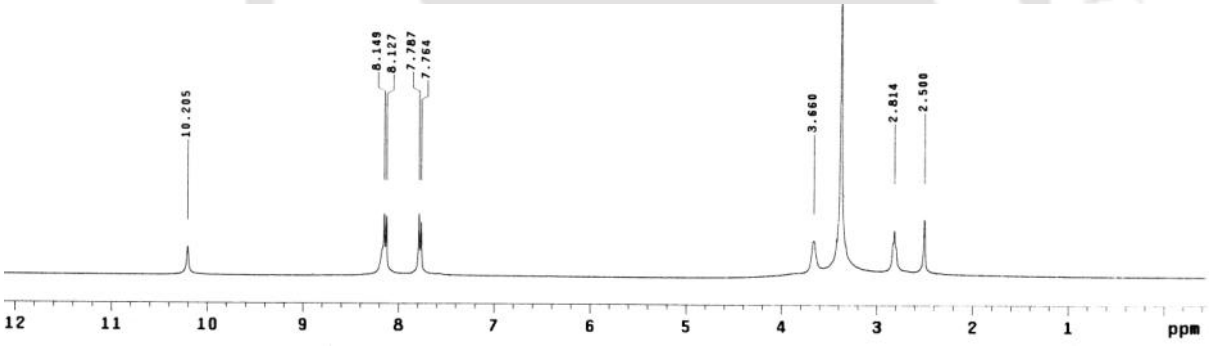

Figure A2.16 ^{1}H NMR spectrum of receptor $\mathbf{L_5}$ (400 MHz, DMSO-d_6).

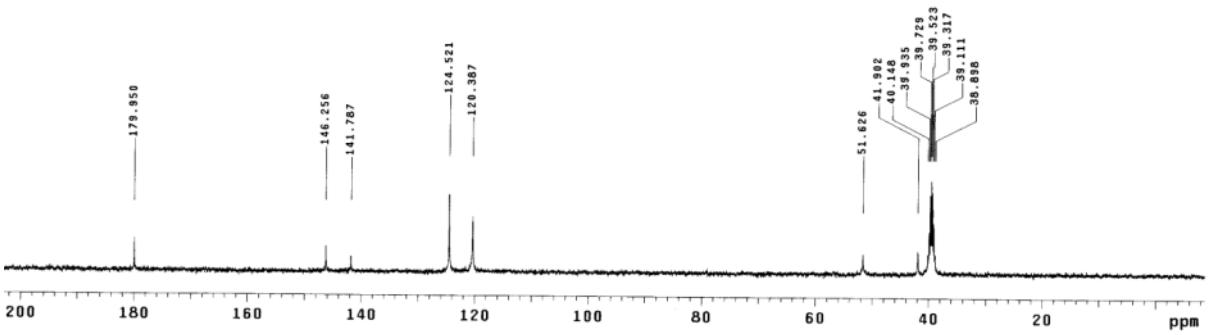

Figure A2.17 ^{13}C NMR spectrum of receptor $\mathbf{L_5}$ (100 MHz, DMSO-d_6).

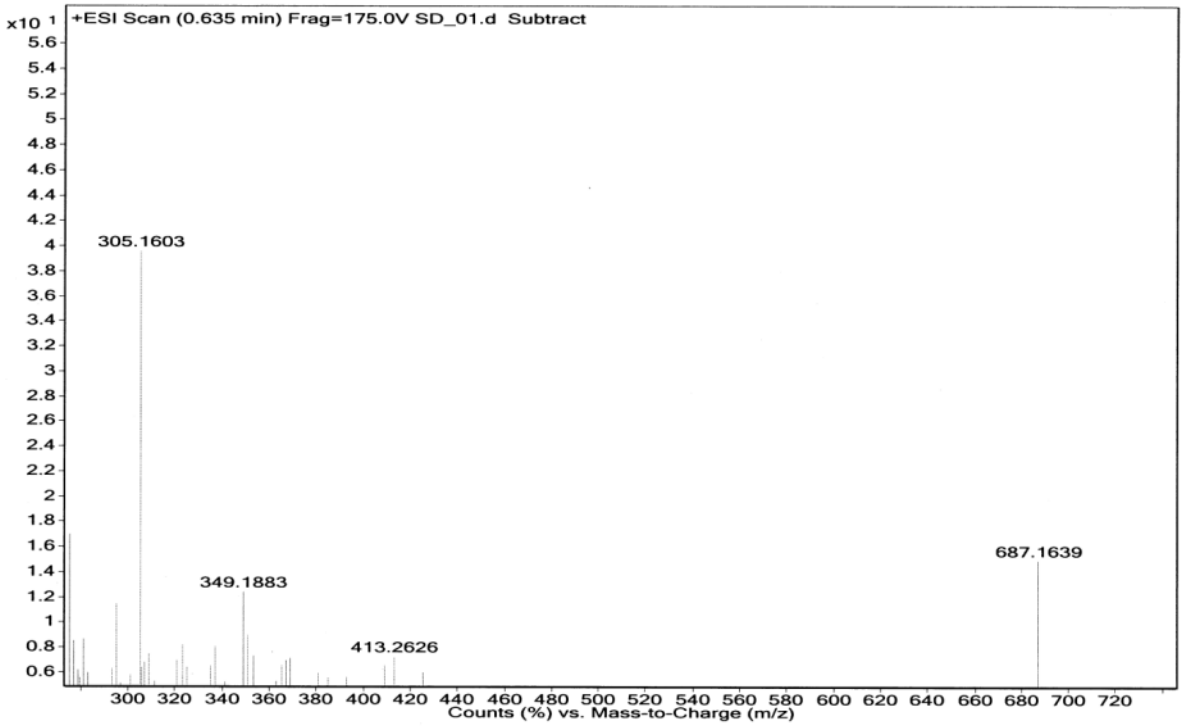

Figure A2.18 ESI-mass spectrum of $\mathbf{L_5}$ showing m/z = 687.164 corresponds to $[M+1]^+$.

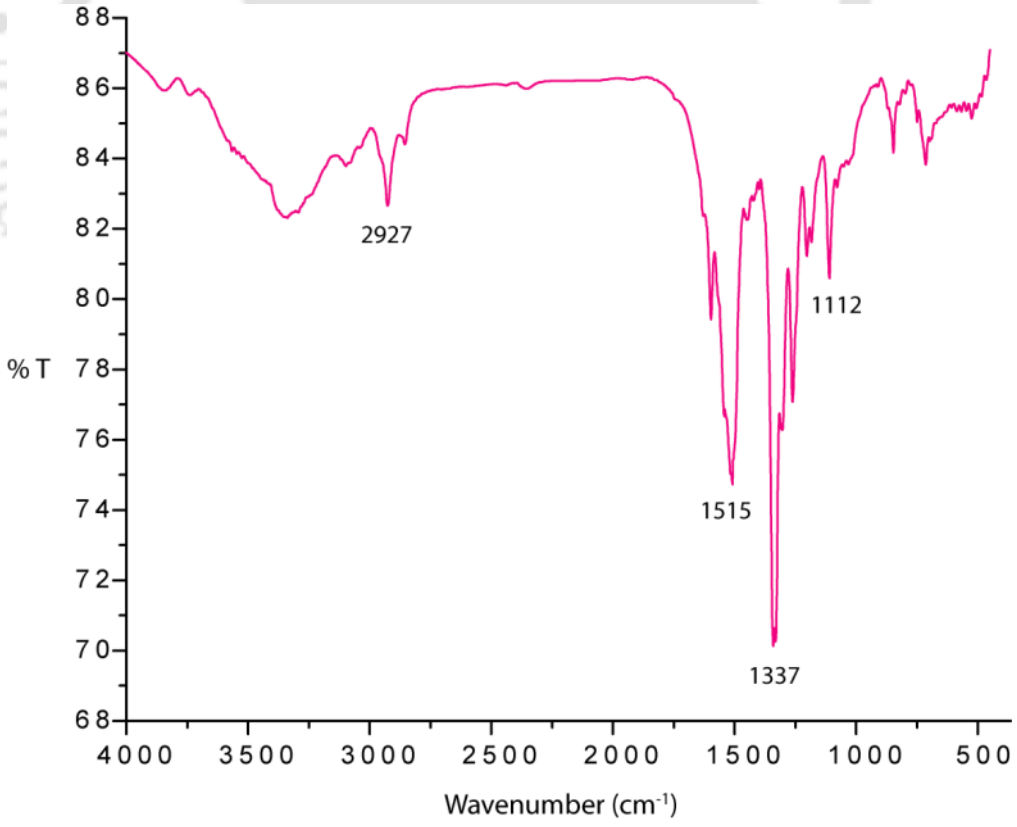

Figure A2.19 FT-IR spectrum of $\mathbf{L_5}$ recorded in KBr pellet.

Characterization data of anion complexes of L_1 (1a-1e):

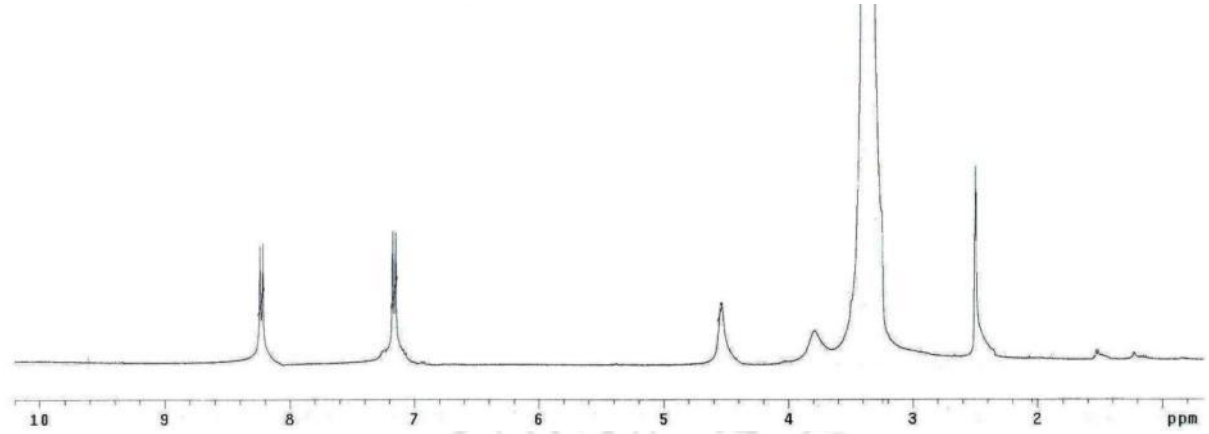

Figure A2.20 ^{1}H NMR spectrum of complex $[(HL_1)^+Cl^-]$, **1a** (400 MHz, DMSO-d_6).

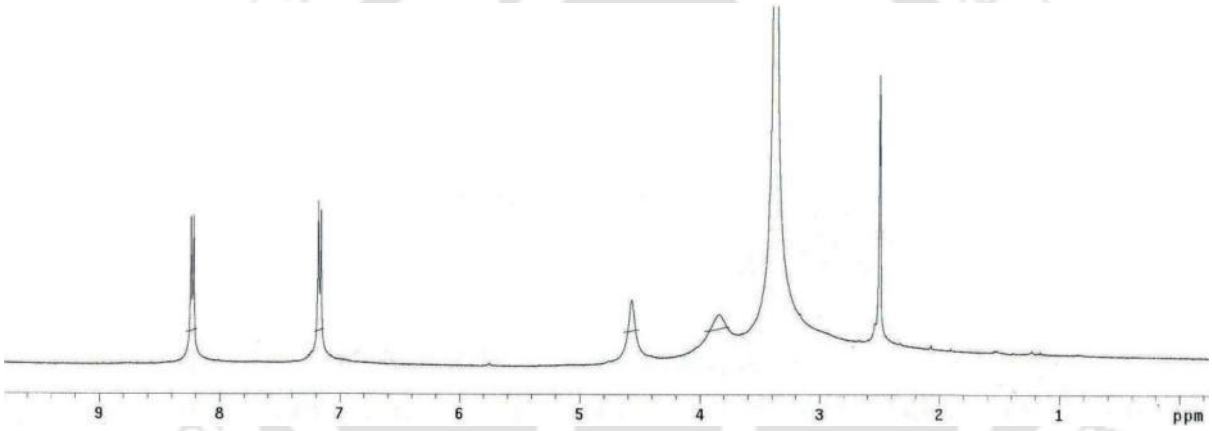

Figure A2.21 ^{1}H NMR spectrum of complex $[(HL_1)^+Br^-]$, **1b** (400 MHz, DMSO-d_6).

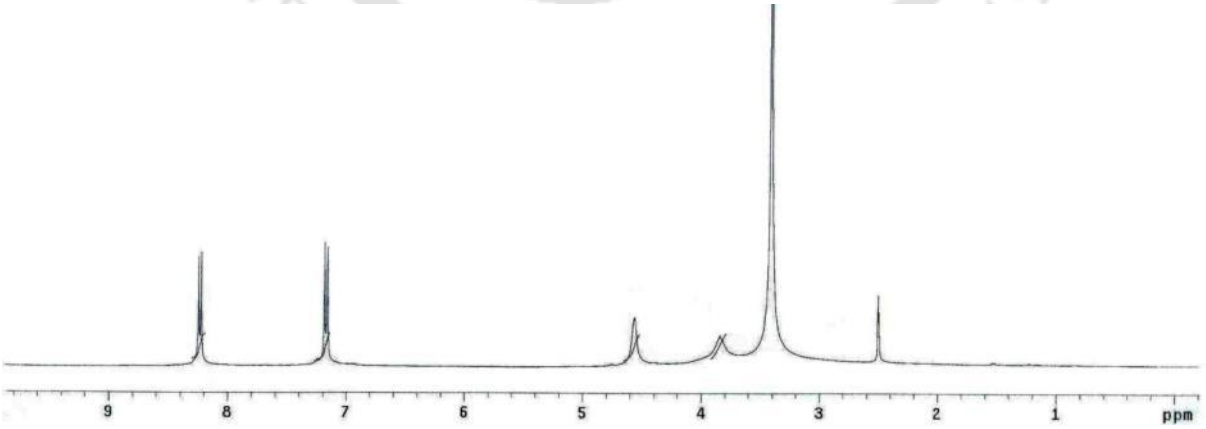

Figure A2.22 ^{1}H NMR spectrum of complex $[(HL_1)^+NO_3^-]$, **1c** (400 MHz, DMSO-d_6).

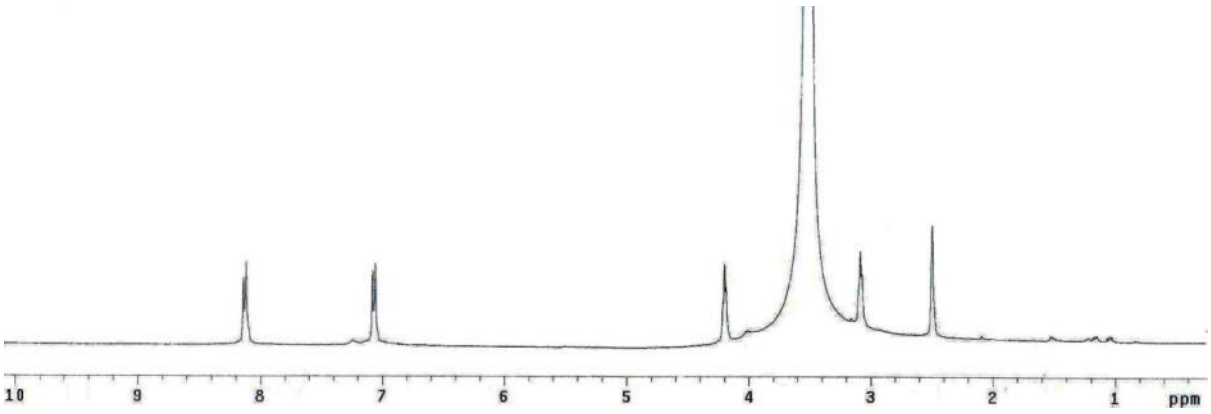

Figure A2.23 ^{1}H NMR spectrum of complex [(H**L**$_1$)$^{+}$$CF_3COO^{-}$], **1d** (400 MHz, DMSO-d_6).

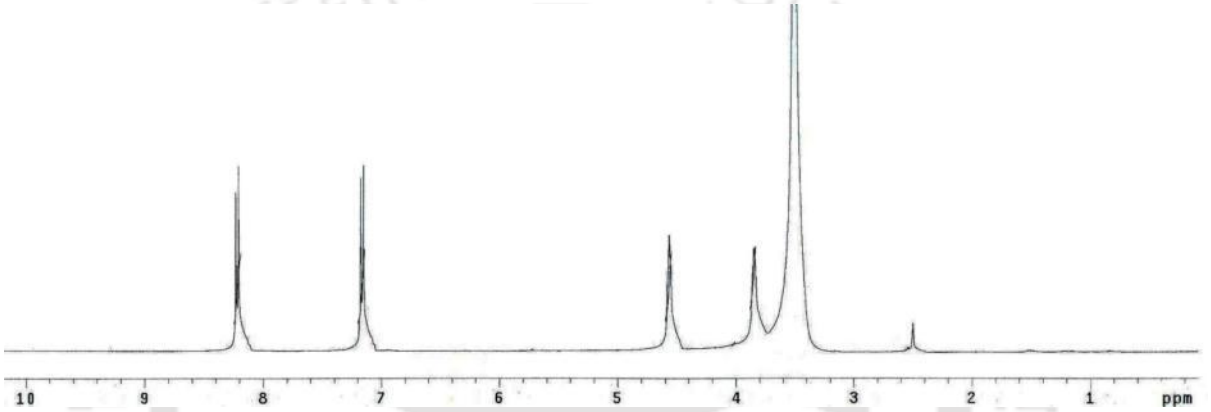

Figure A2.24 ^{1}H NMR spectrum of complex [(H**L**$_1$)$^{+}$$ClO_4^{-}$], **1e** (400 MHz, DMSO-d_6).

Characterization data of anion complexes of L_2 (2a-2d):

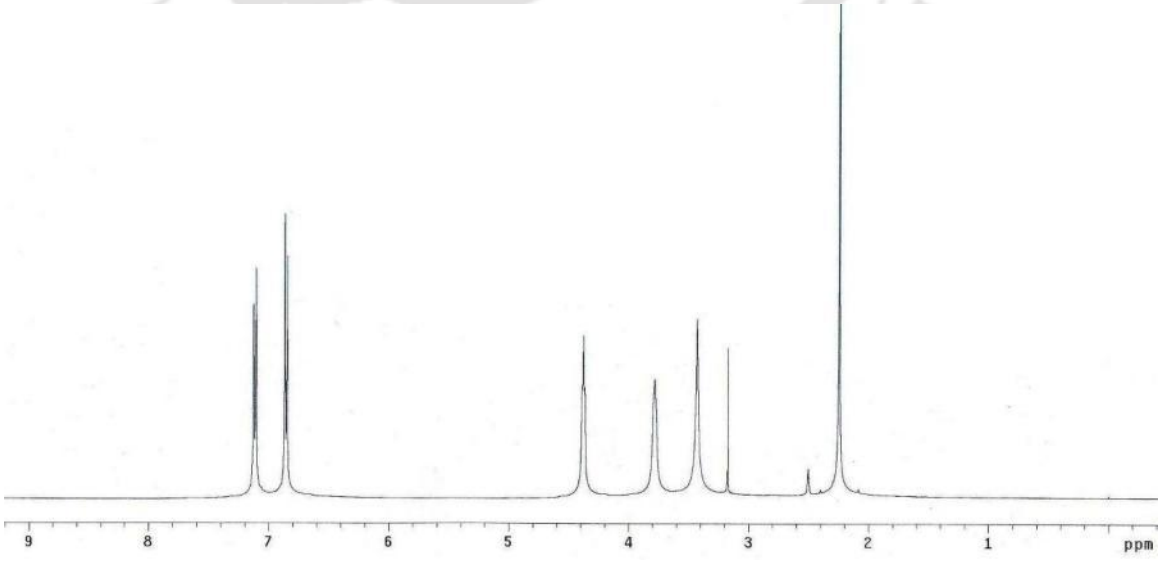

Figure A2.25 ^{1}H NMR spectrum of complex [(H**L**$_2$)$^{+}$$ClO_4^{-}$], **2a** (400 MHz, DMSO-d_6).

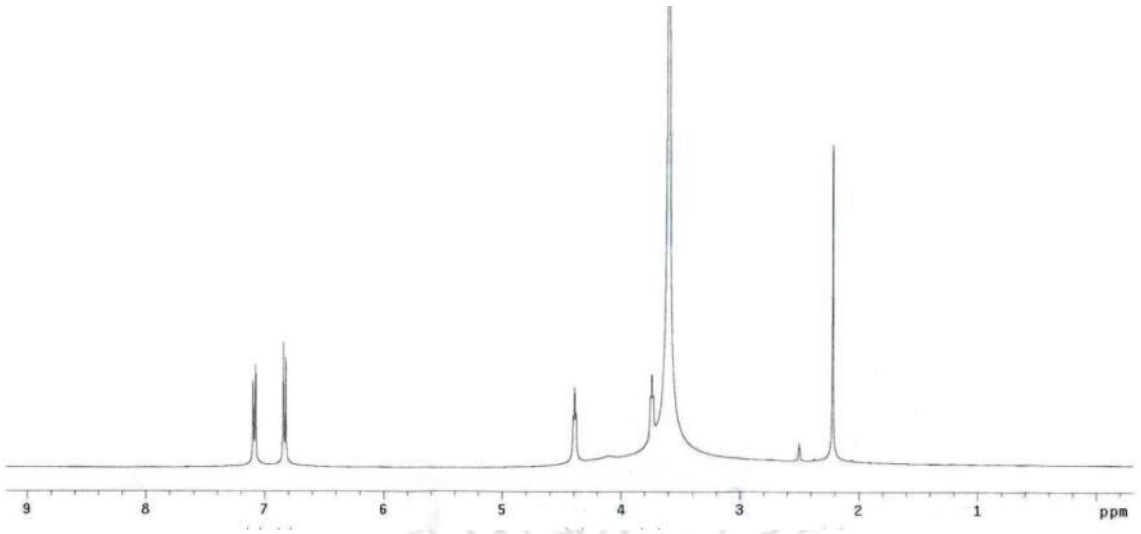

Figure A2.26 ^{1}H NMR spectrum of complex [(H**L**$_2$)$^{+}$Br^{-}]2H$_2$O, **2b** (400 MHz, DMSO-d_6).

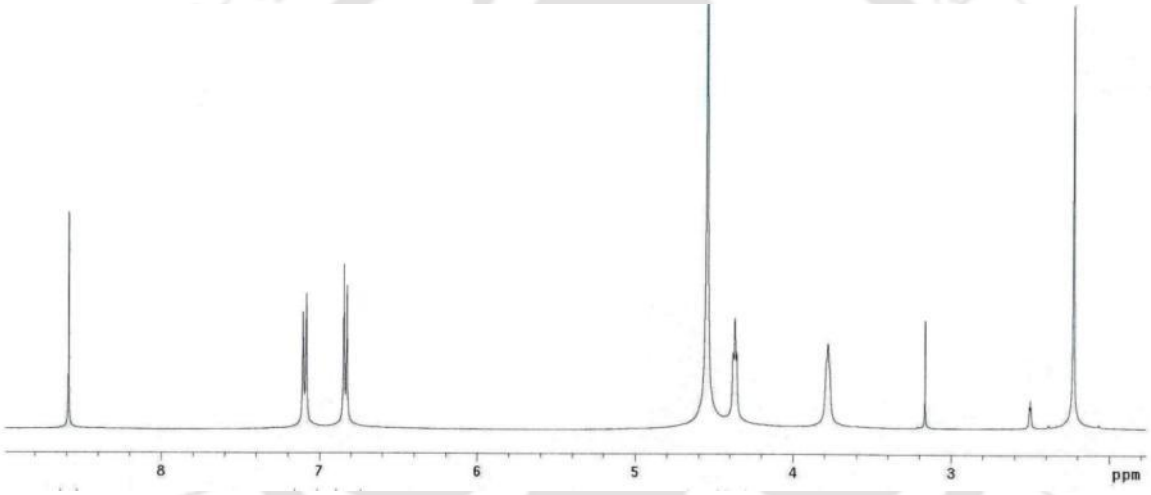

Figure A2.27 ^{1}H NMR spectrum of complex [(H**L**$_2$)$^{+}$PA^{-}], **2c** (400 MHz, DMSO-d_6).

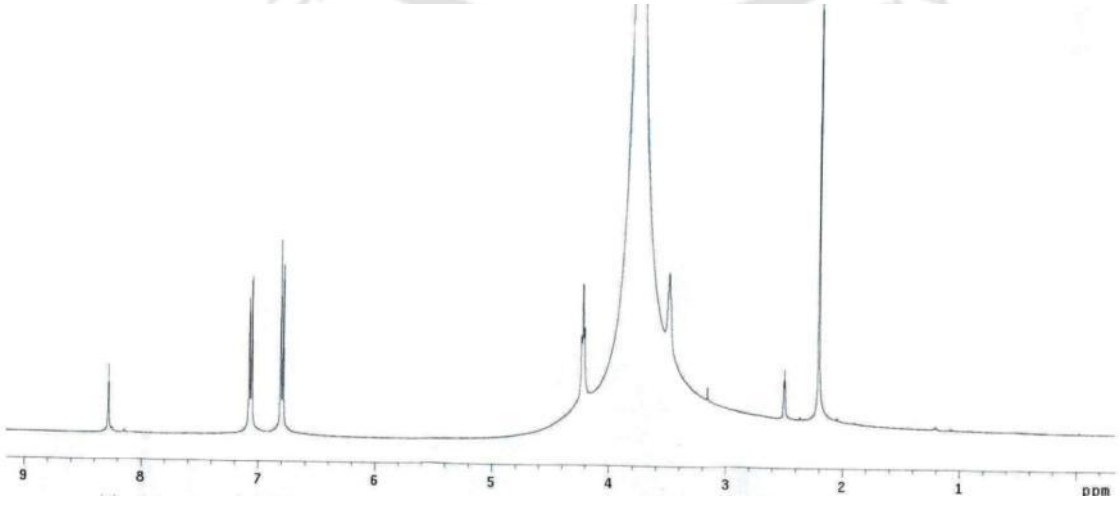

Figure A2.28 ^{1}H NMR spectrum of complex [(H**L**$_2$)$^{+}$PMA^{-}], **2d** (400 MHz, DMSO-d_6).

Characterization data of anion complexes of L_3 (3a-3f):

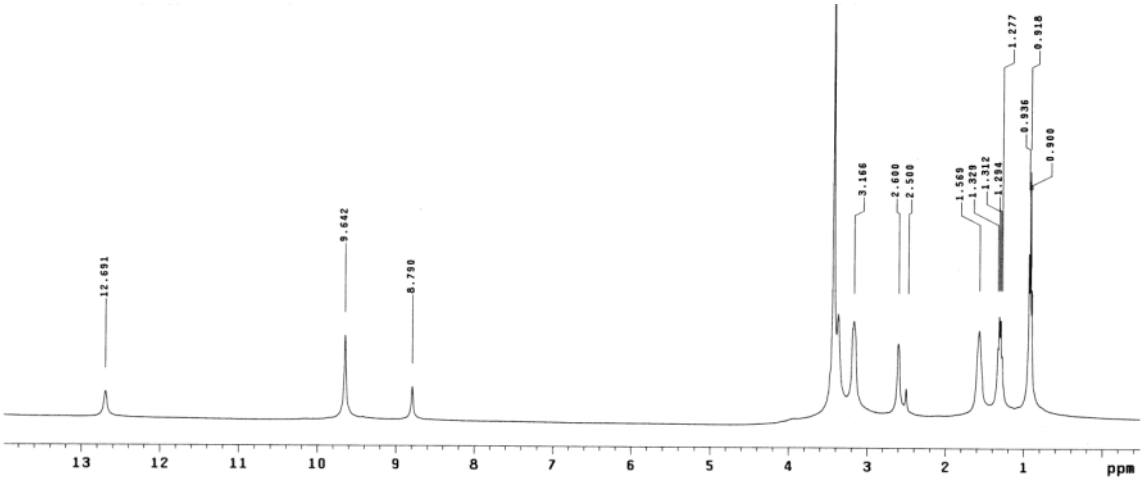

Figure A2.29 ^{1}H NMR spectrum of complex TBA[$\mathbf{L_3}$(F^-)], **3a-IV** (400 MHz, DMSO-d_6).

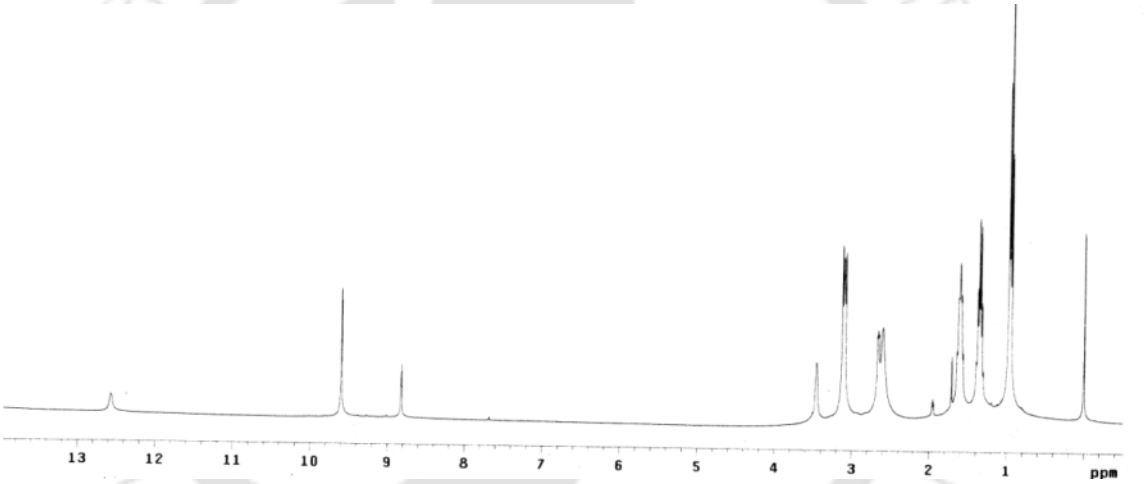

Figure A2.30 ^{1}H NMR spectrum of complex TBA[$\mathbf{L_3}$(F^-)], **3a-IV** (400 MHz, CD_3CN).

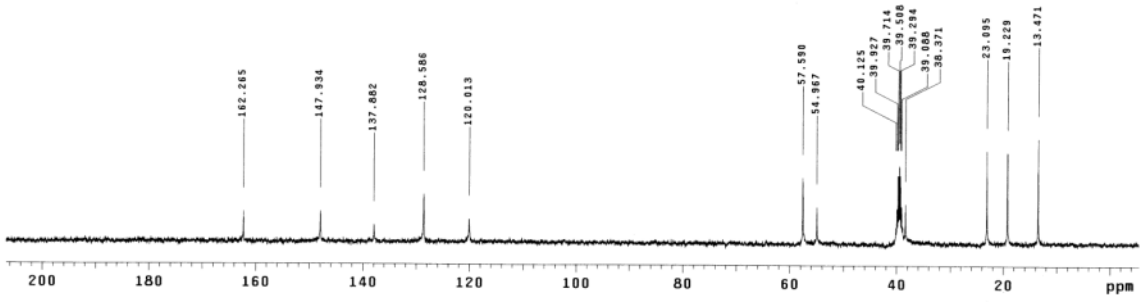

Figure A2.31 ^{13}C NMR spectrum of complex TBA[$\mathbf{L_3}$(F^-)], **3a-IV** (100 MHz, DMSO-d_6).

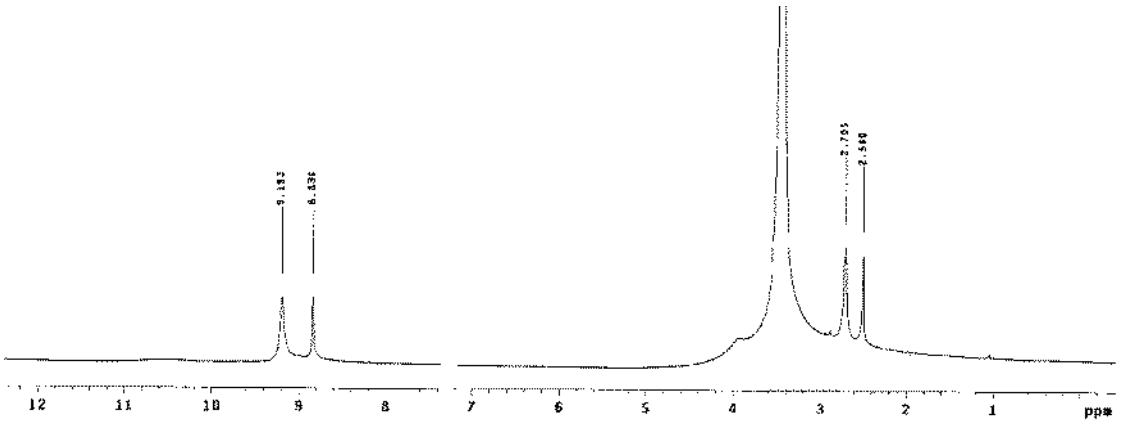

Figure A2.32 ^{1}H NMR spectrum of complex [$\mathbf{L_3}$-2H_2OKF)], **3b** (400 MHz, DMSO-d_6).

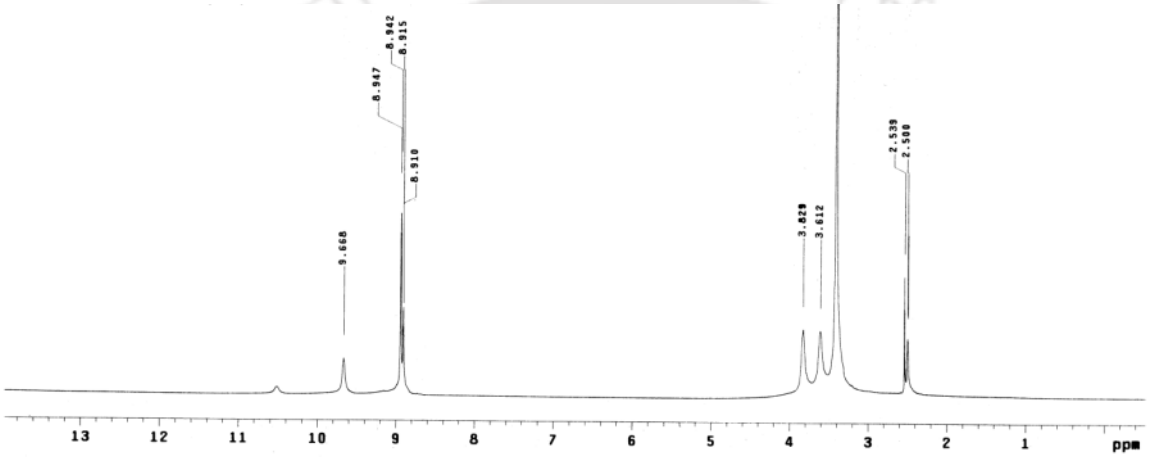

Figure A2.33 ^{1}H NMR spectrum of complex [(H$\mathbf{L_3}$)$^{+}$Cl^{-}], **3c** (400 MHz, DMSO-d_6).

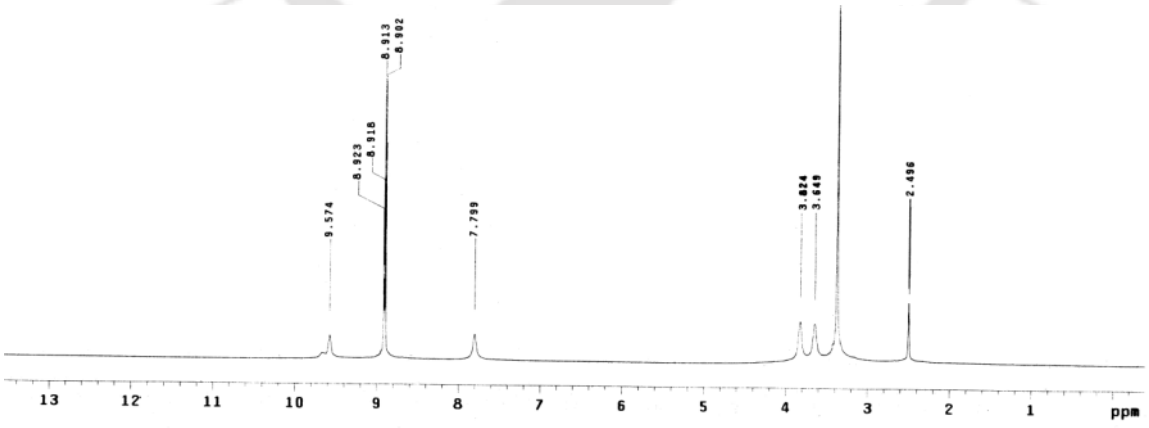

Figure A2.34 ^{1}H NMR spectrum of complex [(H$\mathbf{L_3}$)$^{+}$Br^{-}]2H_2O, **3d** (400 MHz, DMSO-d_6).

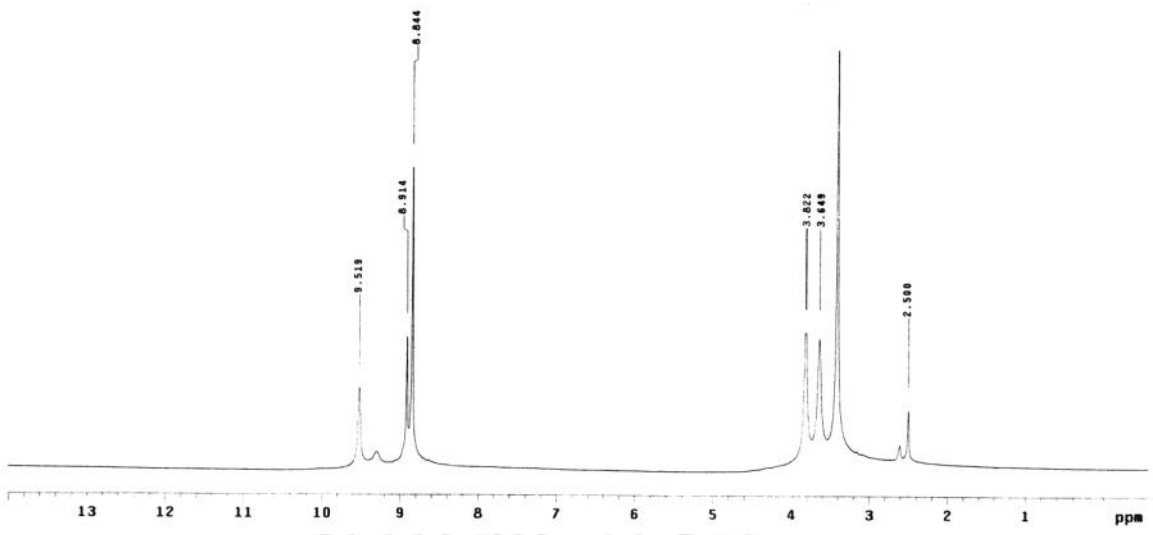

Figure A2.35 ^{1}H NMR spectrum of complex $[(H\mathbf{L_3})^{+}ClO_4^{-}]DMSO{\cdot}H_2O$, **3e** (400 MHz, DMSO-$d_6$).

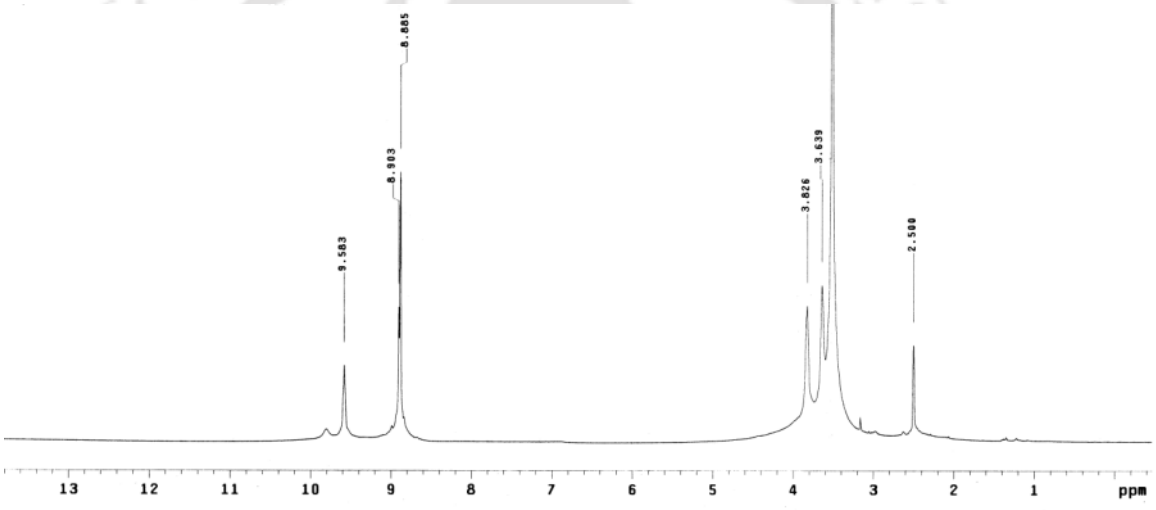

Figure A2.36 ^{1}H NMR spectrum of complex $[(H\mathbf{L_3})^{+}HSO_4^{-}]DMSO$, **3f** (400 MHz, DMSO-$d_6$).

Characterization data of anion complexes of L_4 (4a and 4b):

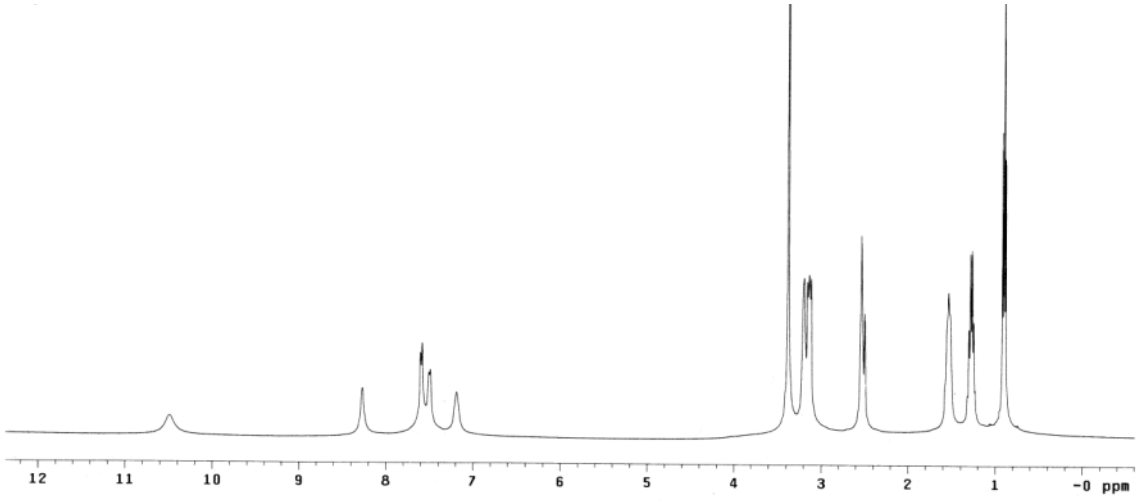

Figure A2.37 ^{1}H NMR spectrum of complex 2TBA[2$\mathbf{L_4}$(CO_3)], **4a** (400 MHz, DMSO-d_6).

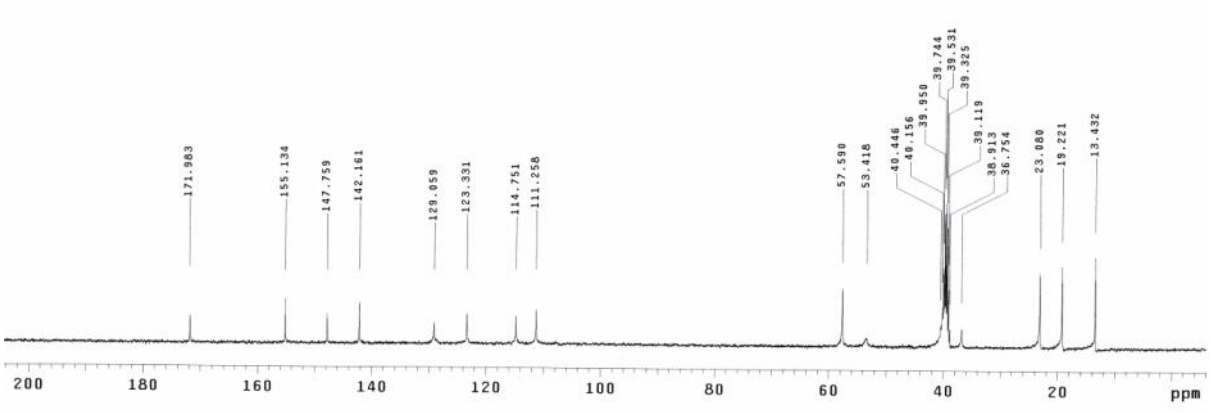

Figure A2.38 ^{13}C NMR spectrum of complex 2TBA[2$\mathbf{L_4}$(CO_3)], **4a** (100 MHz, DMSO-d_6).

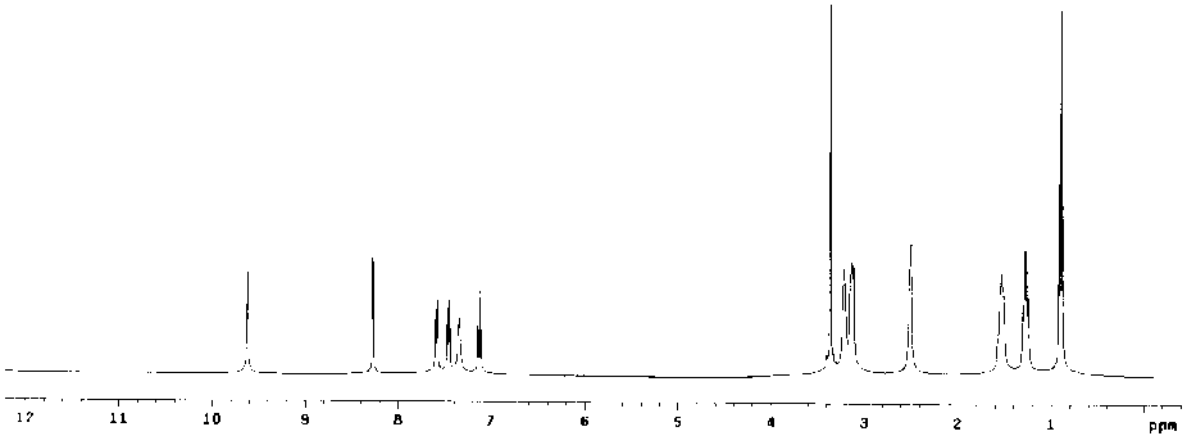

Figure A2.39 ^{1}H NMR spectrum of complex 2TBA[2$\mathbf{L_4}$(SO_4)], **4b** (400 MHz, DMSO-d_6).

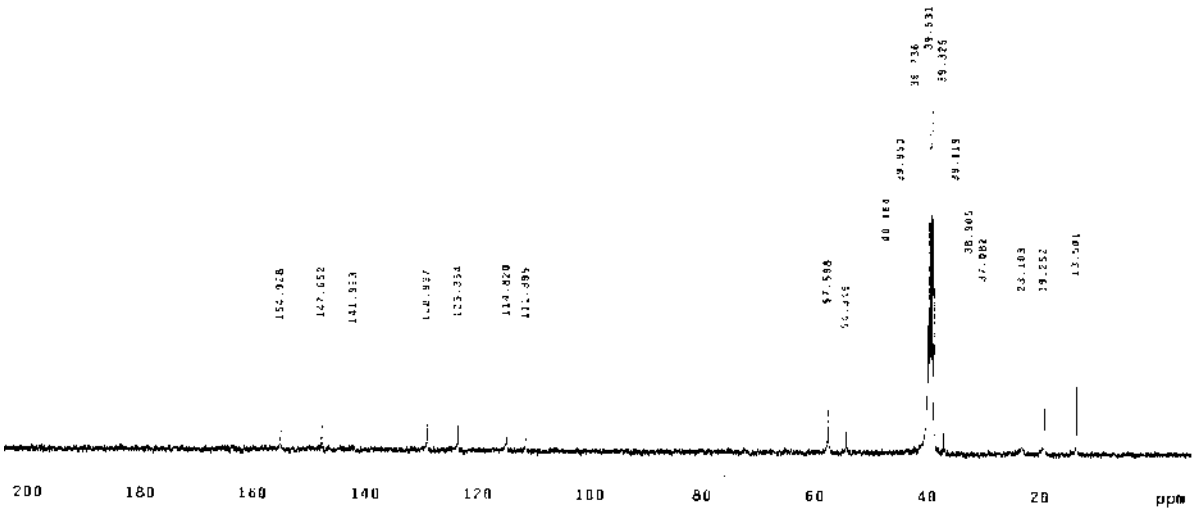

Figure A2.40 ^{13}C NMR spectrum of complex 2TBA[2**L**$_4$(SO_4)], **4b** (100 MHz, DMSO-d_6).

Characterization data of anion complexes of L_5 (5a-5f):

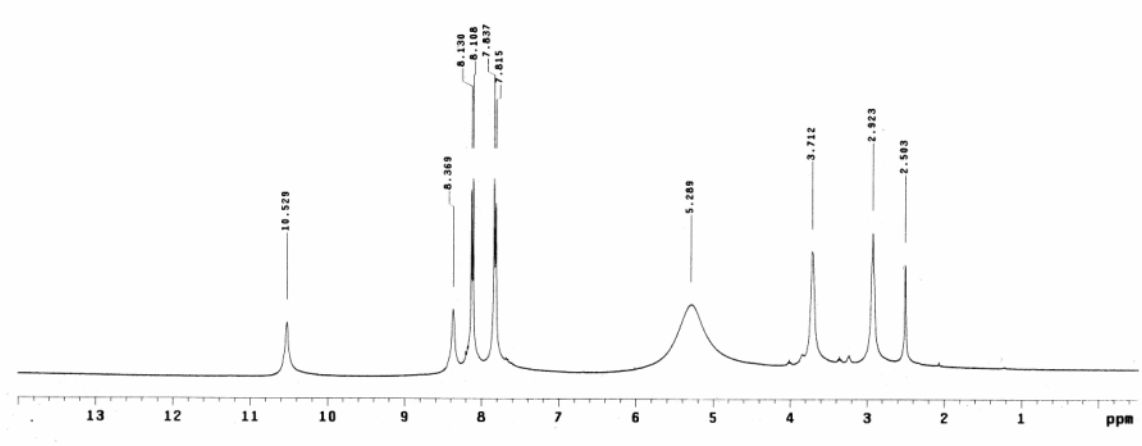

Figure A2.41 ^{1}H NMR spectrum of complex [2(H**L**$_5$)$^+$-HPO_4^{2-})]3H_2O, **5a** (400 MHz, DMSO-d_6).

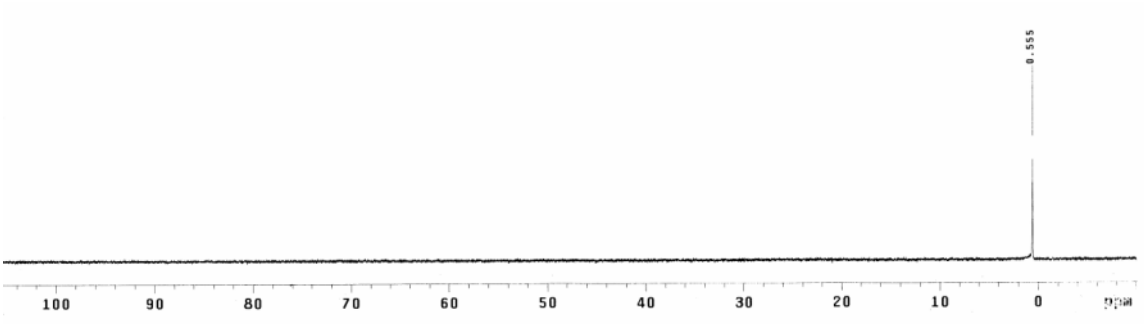

Figure A2.42 ^{31}P NMR spectrum of complex [2(H**L**$_5$)$^+$-HPO_4^{2-})]3H_2O, **5a** (400 MHz, DMSO-d_6).

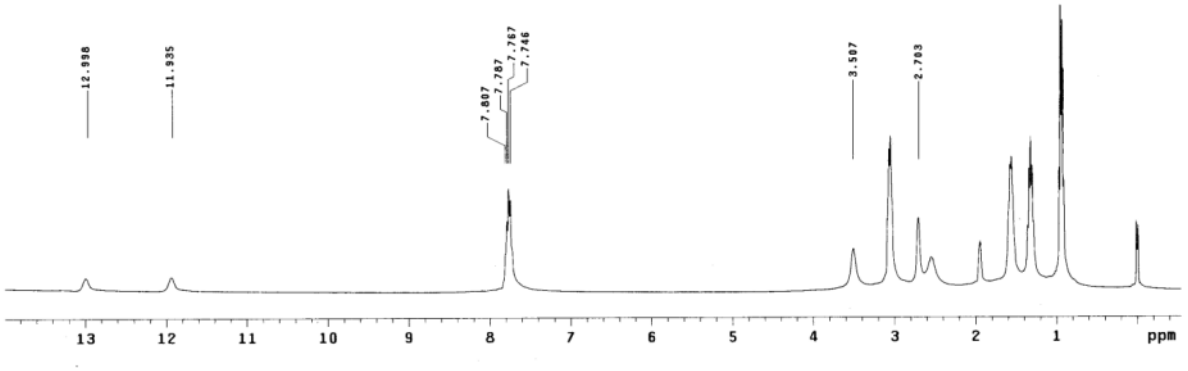

Figure A2.43 ^{1}H NMR spectrum of complex 3TBA[2$\mathbf{L}_5$(PO_4)]2MeCN, **5b-I** (400 MHz, DMSO-d_6).

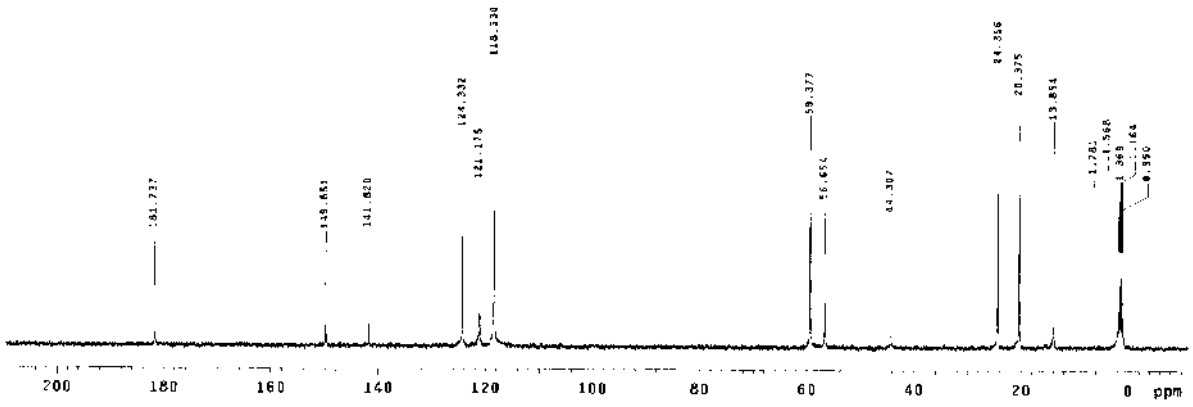

Figure A2.44 ^{13}C NMR spectrum of complex 3TBA[2$\mathbf{L}_5$(PO_4)]2MeCN, **5b-I** (100 MHz, DMSO-d_6).

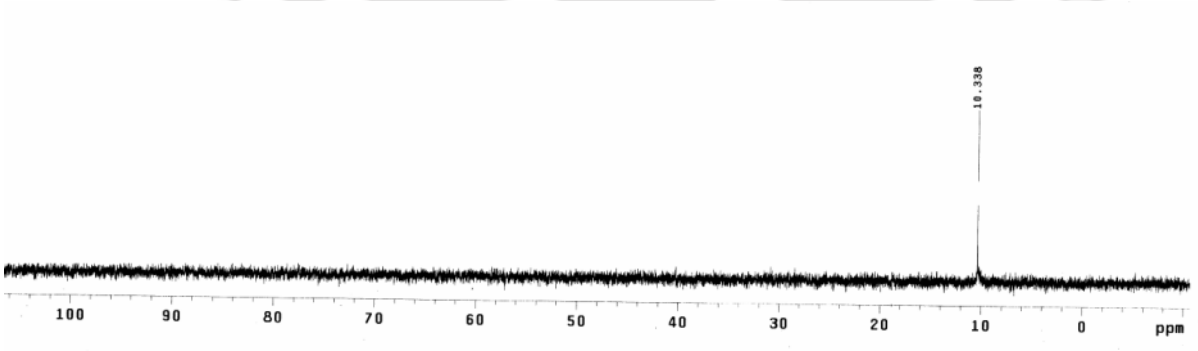

Figure A2.45 ^{31}P NMR spectrum of complex 3TBA[2$\mathbf{L}_5$(PO_4)]2MeCN, **5b-I** (400 MHz, DMSO-d_6).

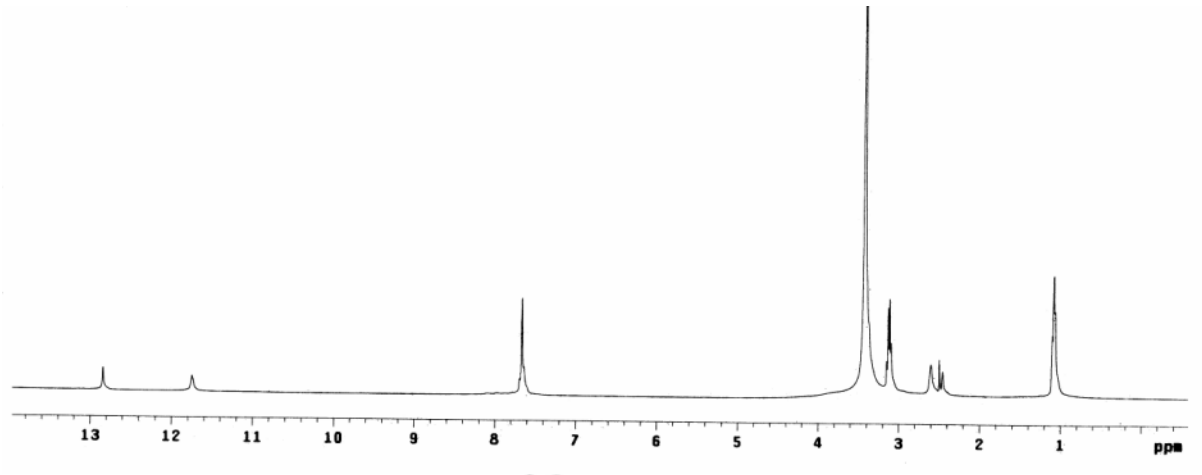

Figure A2.46 ^{1}H NMR spectrum of complex 3TEA[2**L**$_5$(PO$_4$)], **5b-II** (400 MHz, DMSO-d_6).

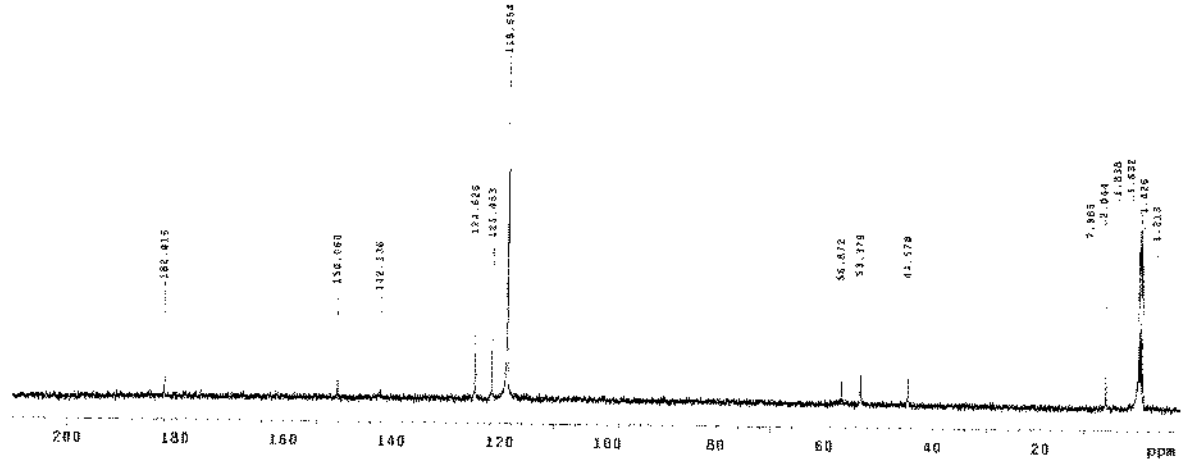

Figure A2.47 ^{13}C NMR spectrum of complex 3TEA[2**L**$_5$(PO$_4$)], **5b-II** (100 MHz, CD$_3$CN).

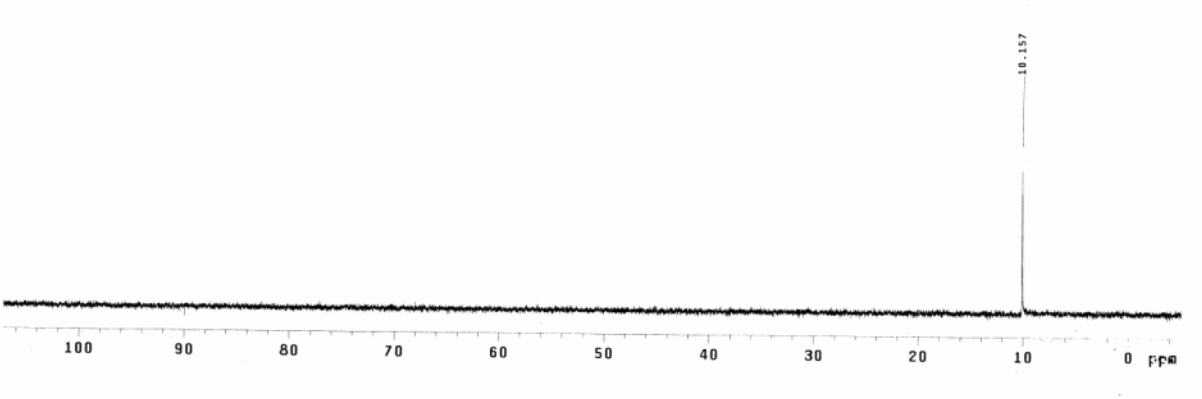

Figure A2.48 ^{31}P NMR spectrum of complex 3TEA[2**L**$_5$(PO$_4$)], **5b-II** (400 MHz, DMSO-d_6).

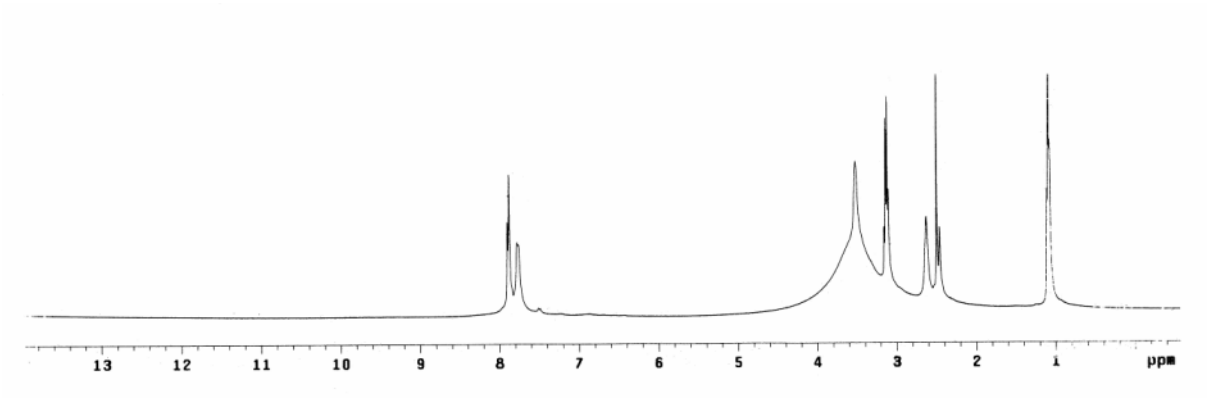

Figure A2.49 ^{1}H NMR spectrum of complex 2TEA[2$\mathbf{L}_5(CO_3)$], **5c** (400 MHz, DMSO-d_6).

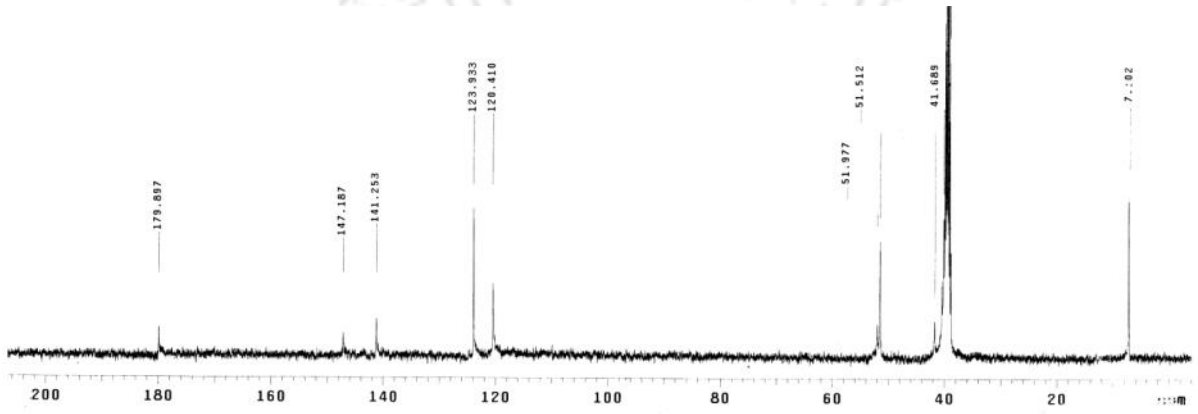

Figure A2.50 ^{13}C NMR spectrum of complex 2TEA[2$\mathbf{L}_5(CO_3)$], **5c** (100 MHz, DMSO-d_6).

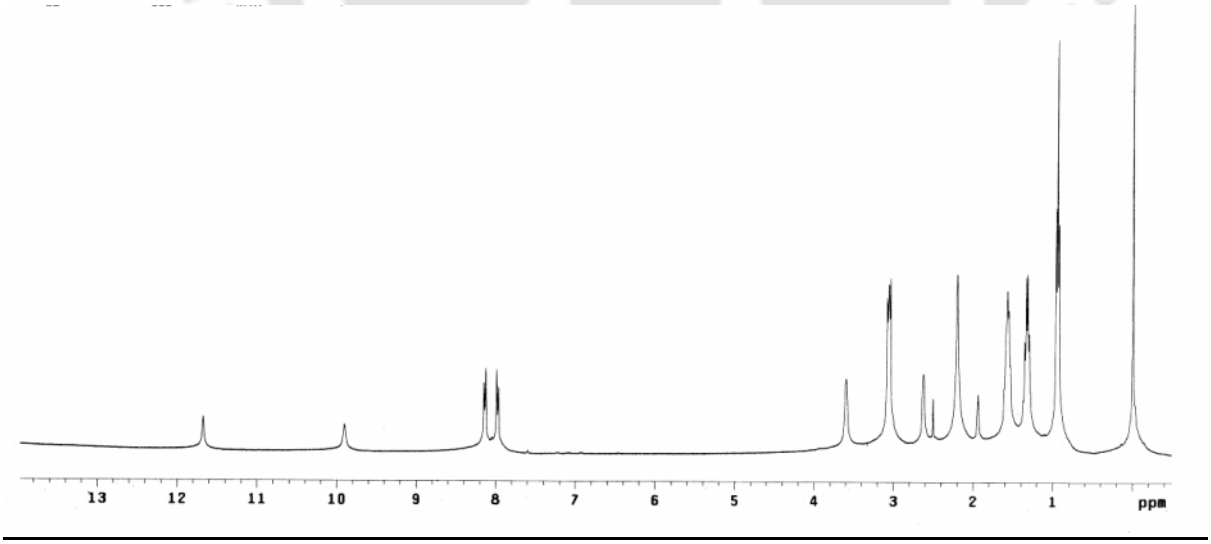

Figure A2.51 ^{1}H NMR spectrum of complex 2TBA[$\mathbf{L}_5(SO_4)$], **5d** (400 MHz, DMSO-d_6).

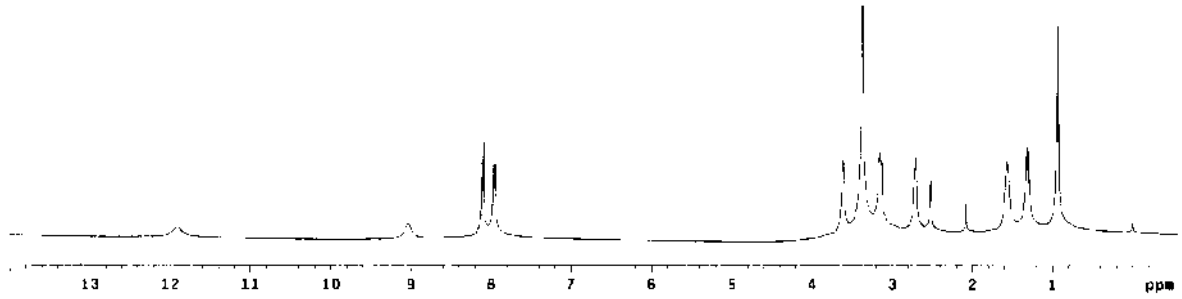

Figure A2.52 ^{1}H NMR spectrum of complex TBA[**L**$_5$(F)]2DMSO, **5e-I** (400 MHz, CD_3CN).

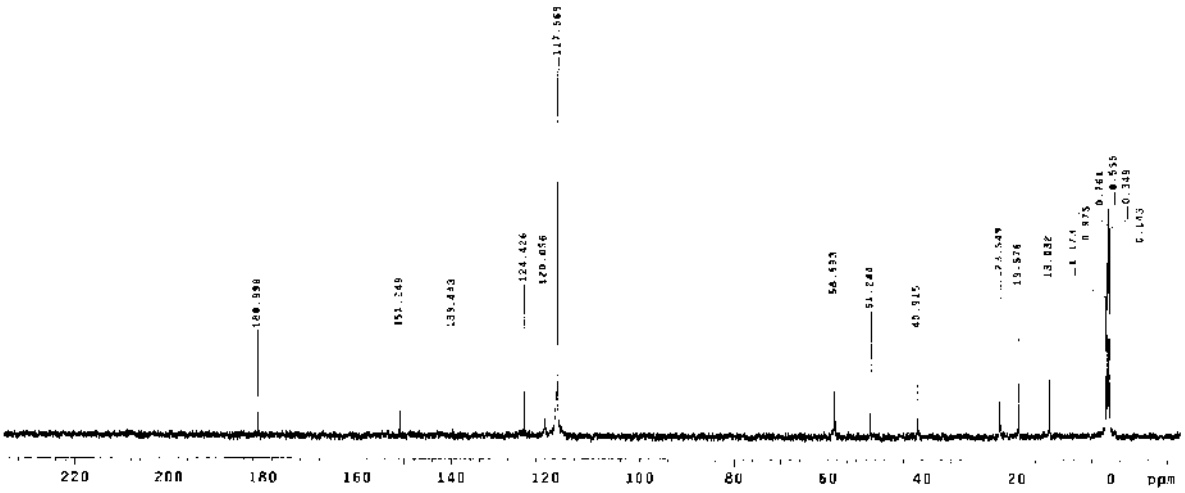

Figure A2.53 ^{13}C NMR spectrum of complex TBA[**L**$_5$(F)]2DMSO, **5e-I** (100 MHz, CD_3CN).

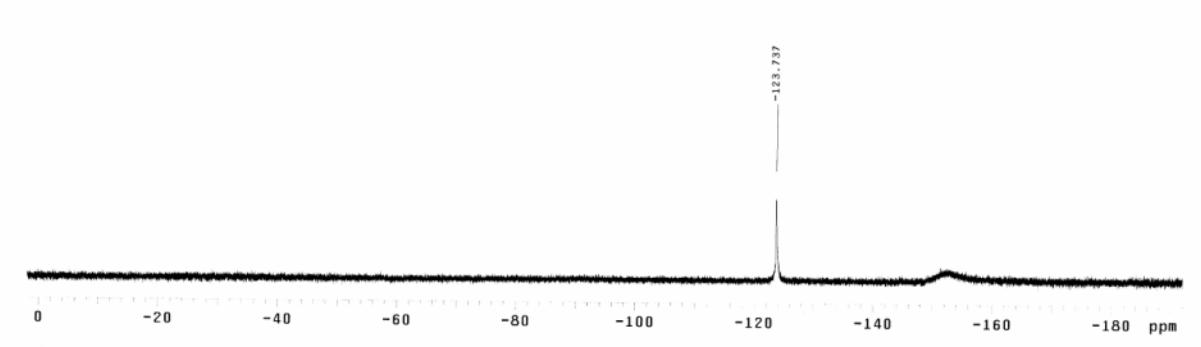

Figure A2.54 ^{19}F NMR spectrum of complex TBA[**L**$_5$(F)]2DMSO, **5e-I** (400 MHz, CD_3CN).

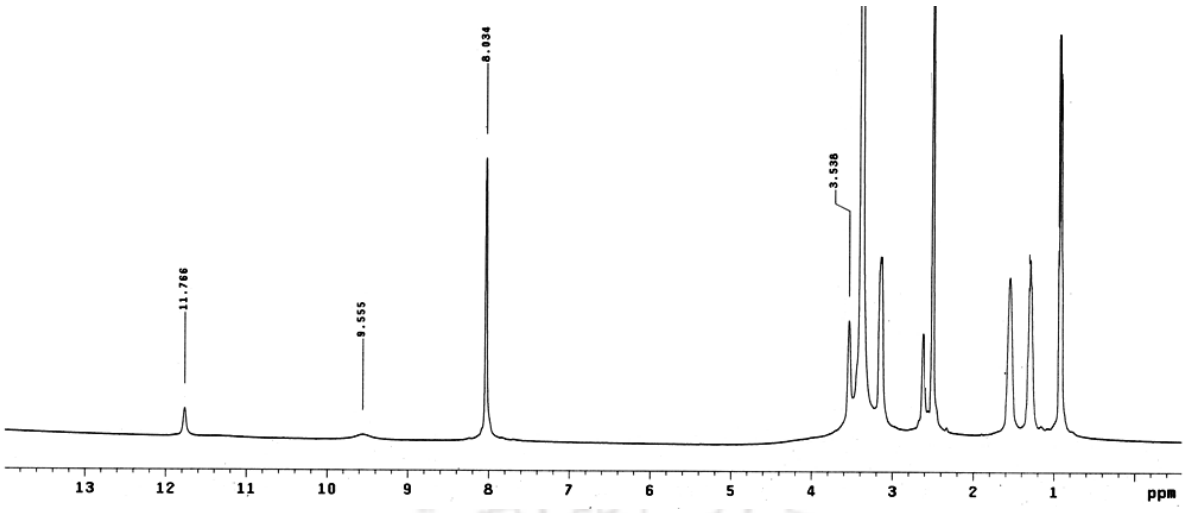

Figure A2.55 ^{1}H NMR spectrum of complex TBA[$\mathbf{L}_5$(F)]MeCN, **5e-II** (400 MHz, DMSO-d_6).

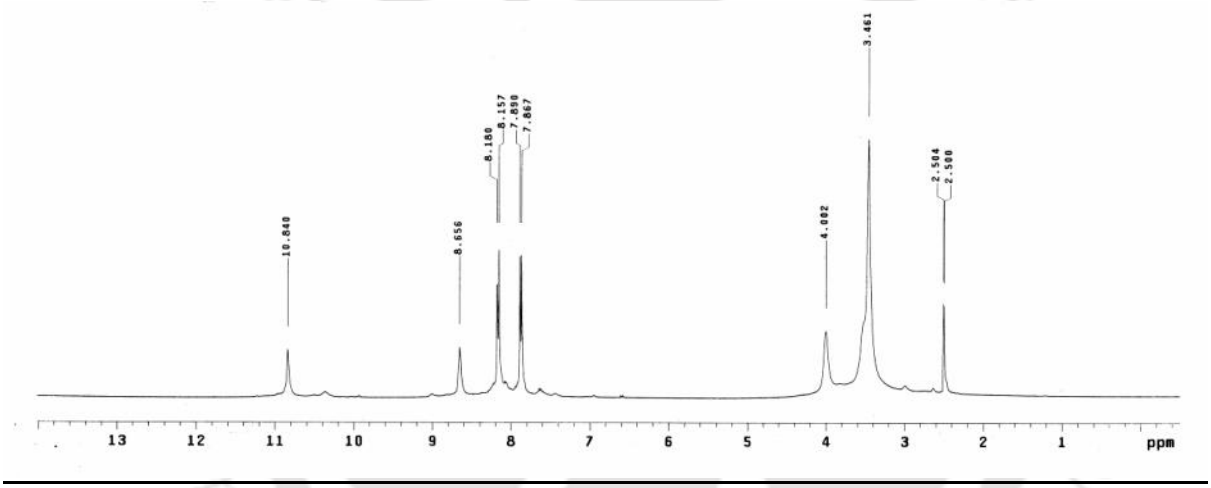

Figure A2.56 ^{1}H NMR spectrum of complex [($\mathbf{HL}_5$)$^{+}$Cl^{-})]DMF, **5f** (400 MHz, DMSO-d_6).

Annexure 3

Table A3.1 Intermolecular noncovalent interactions in polymorphs **I**, **II** and **III**.

D-H···A	*d*(H···A) (Å)	*d*(D···A) (Å)	∠(DHA) (deg)
Polymorph-**I**			
C24-H···O3	2.674	3.557	158.63
C17-H(A)···O5	2.566	3.520	167.72
C4-H···O6	2.596	3.283	131.03
C8-H···O8	2.431	3.156	134.86
C15-H···O9	2.629	3.424	143.80
C23-H···O9	2.570	3.135	119.51
Polymorph-**II**			
C8-H···O6	2.443	3.349	164.28
C9-H(A)···O8	2.587	3.506	158.35
C16-H···O9	2.684	3.549	155.24
Polymorph-**III**			
C5-H···O8	2.515	3.285	140.27
C2-H(A)···O5	2.515	3.373	147.29
C2-H(B)···O5	2.672	3.275	120.66
C10-H(A)···O3	2.629	3.399	136.50
C16-H···O3	2.631	3.221	121.87

Table A3.2 Polymorph Screening of podand $\mathbf{L_1}$.

Solvent(s)	**Polymorph**
DMSO	**I**
Acetonitrile	**I**
Ethanol	**I/II**
Methanol	**I/II**
Ethyl acetate	**I/II**
DCM	**I/II**
Chloroform	**I/II**
THF	**I/II**
Ethanol/Acetic acid (3:1)	**II**
DMSO/Acetic acid (3:1)	**III**
Ethanol (refluxed and cooled)	**III**

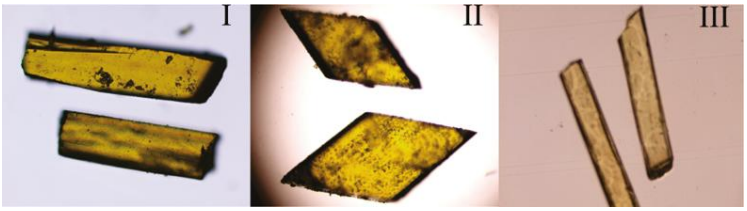

Figure A3.1 Crystal habit of polymorphs **I**, **II** and **III**.

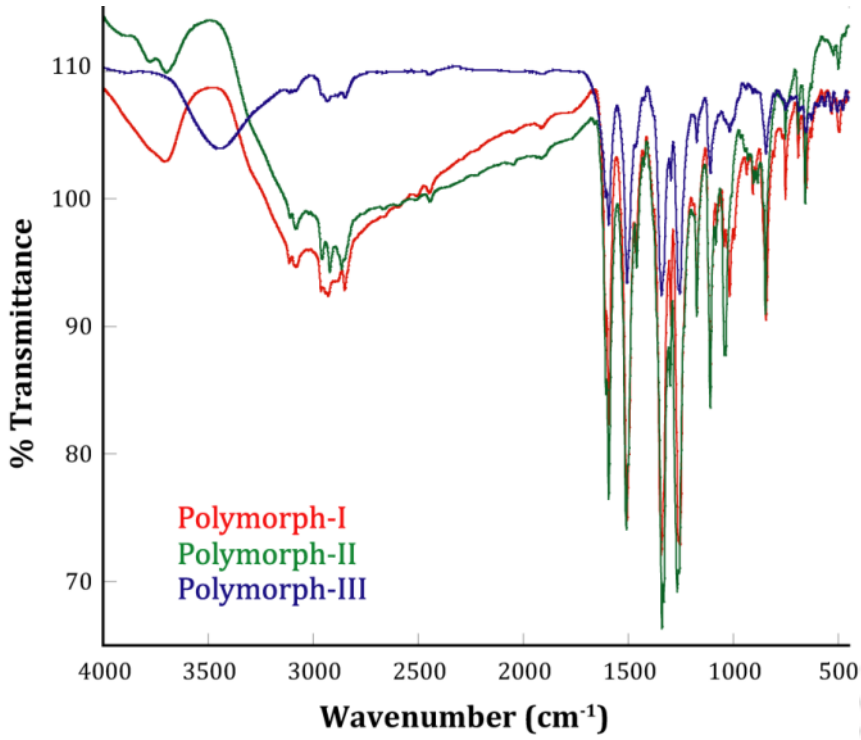

Figure A3.2 FT-IR spectra of polymorphs **I**, **II** and **III**.

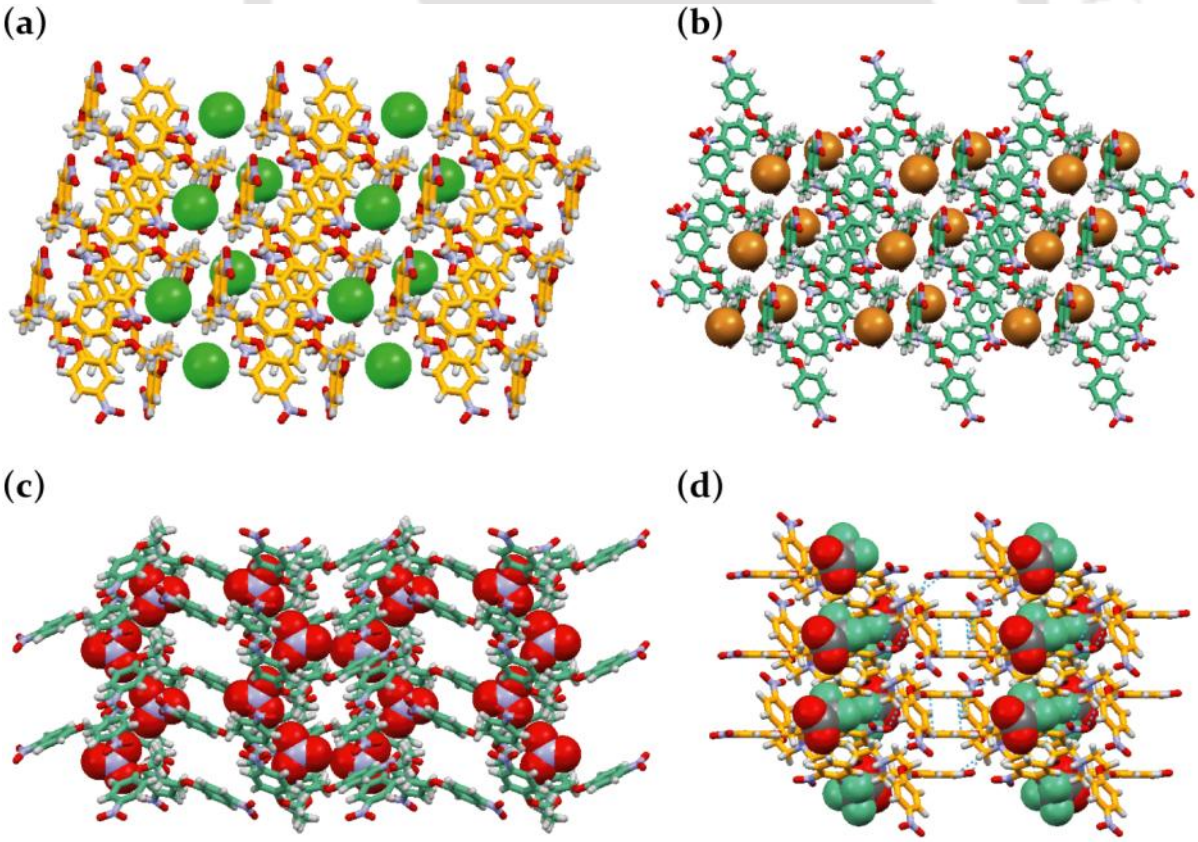

Figure A3.3 Crystal packing diagrams of anion complexes of protonated $\mathbf{L_1}$, **1a-1d**.

Table A3.3 Intermolecular C–H···O-(nitro), C–H···π and π-stacking interactions in anion complexes of protonated $\mathbf{L_1}$ (**1a**-**1e**).

Complexes	D-H···A	*d*(H···A) (Å)	*d*(D···A) (Å)	∠(DHA) (°)
1a	C16-H···O2	2.51	3.390	156
	C2-H(B)···O3	2.60	3.229	121
	C10-H(A)···O3	2.59	3.560	178
	C8-H···O3	2.33	3.222	160
	C17-H(B)···O5	2.70	3.349	124
	C20-H···O6	2.52	3.428	164
	C7-H···C2g	3.03	3.970	157
	C1g···C1g		4.183	
	C3g···C3g		3.610	
	C1g···C3g		3.858	
1b	C24-H···O3	2.63	3.499	162
	C2-H(A)···O5	2.55	3.559	172
	C10-H(A)···O5	2.59	3.263	125
	C16-H···O5	2.42	3.328	163
	C8-H···O6	2.52	3.415	160
	C23-H···O9	2.70	3.504	150
	C15-H···C1g	3.05	3.924	156
	C3g···C3g		3.601	
	C3g···C2g		3.906	
1c	C1-H(B)···O3	2.70	3.594	152
	C24-H···O3	2.60	3.323	134
	C2-H(A)···O5	2.60	3.472	148
	C17-H(B)···O5	2.67	3.644	175
	C4-H···O6	2.48	3.399	168
	C10-H(A)···O6	2.58	3.256	126
	C8-H···O9	2.40	3.089	130
1d	C9-H(A)···O2	2.56	3.324	135
	C10-H(A)···O3	2.67	3.620	164
	C17-H(B)···O5	2.68	3.615	160
	C17-H(B)···O6	2.66	3.497	143
	C20-H···O6	2.56	3.155	121
	C1g···C1g		3.726	
	C2g···C2g		3.518	
1e	C17-H(A)···O2	2.54	3.367	142
	C10-H(B)···O3	2.71	3.594	151
	C17-H(B)···O3	2.33	3.235	154
	C9-H(B)···O5	2.51	3.373	147
	C24-H···O6	2.54	3.431	144
	C8-H···O8	2.68	3.563	157

Annexure 4

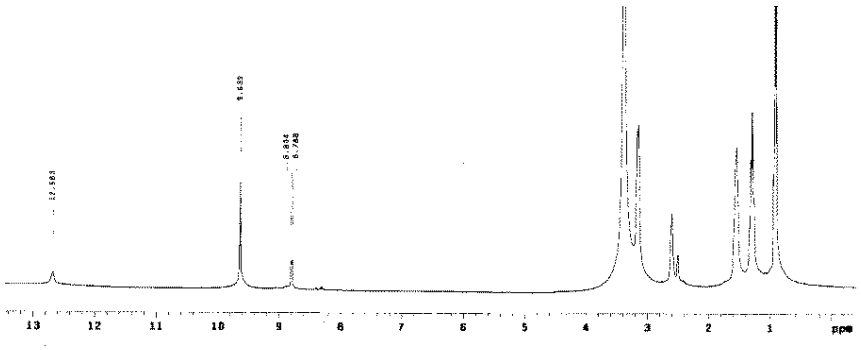

Figure A4.1 ^{1}H NMR spectrum of $\mathbf{L_3}$ (DMSO-d_6) in presence of equivalent amount of TBAF.

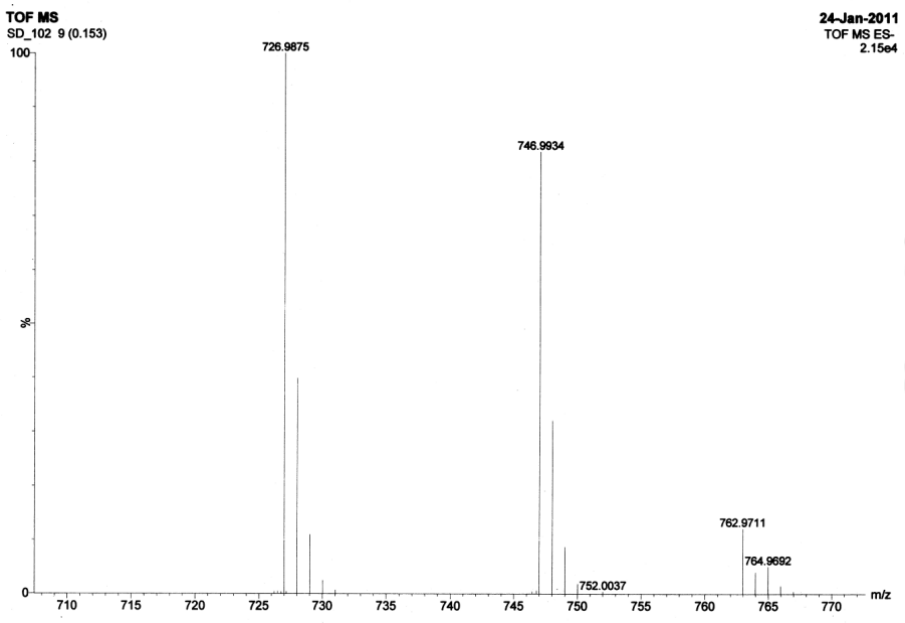

Figure A4.2 ESI-mass spectrum of $\mathbf{L_3}$ in presence of excess TBAF in acetonitrile (MeCN) showing *m/z* = 746.99 for the fluoride-encapsulated complex.

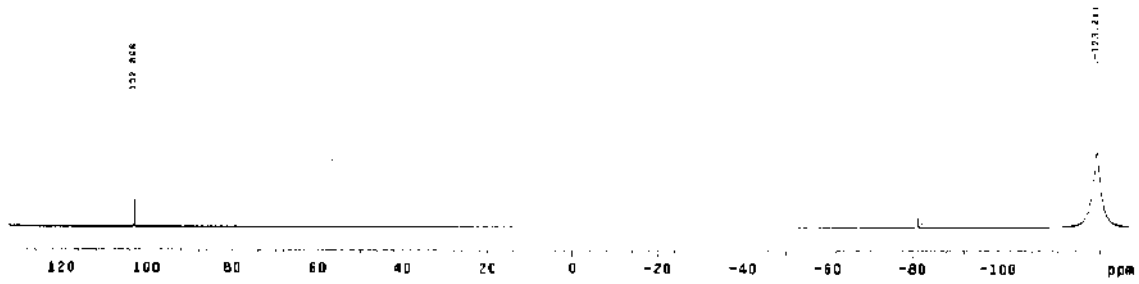

Figure A4.3 ^{19}F NMR spectrum of TBAF in DMSO-d_6.

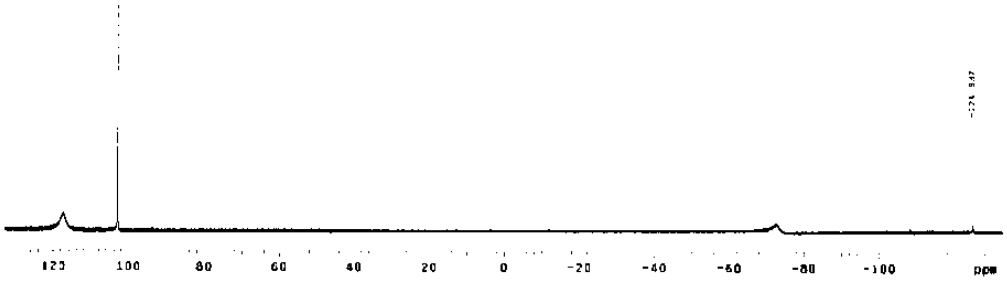

Figure A4.4 ^{19}F NMR spectrum of TBAF (DMSO-d_6) in presence of equivalent amount of $\mathbf{L_3}$.

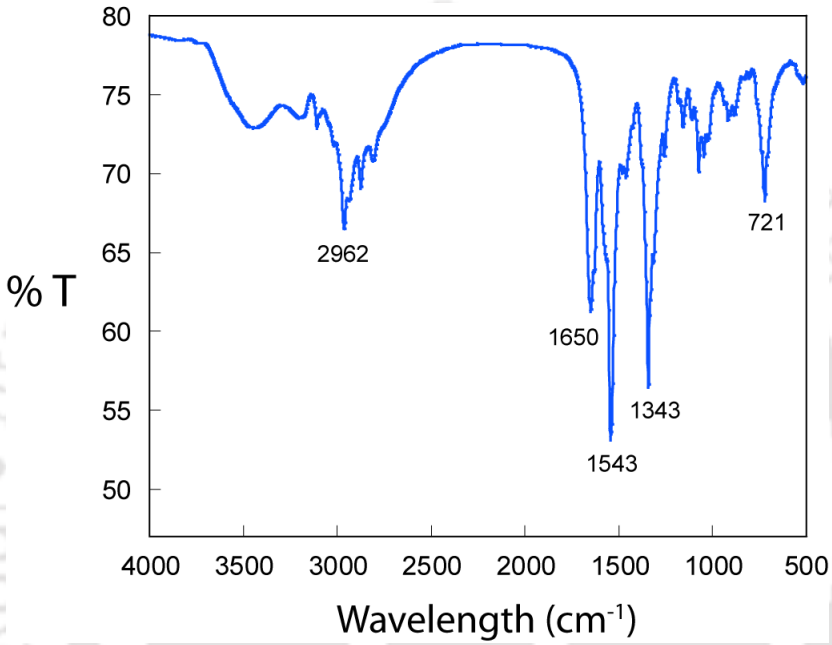

Figure A4.5 FT-IR spectrum of solvate **3a-I** recorded in KBr pellet.

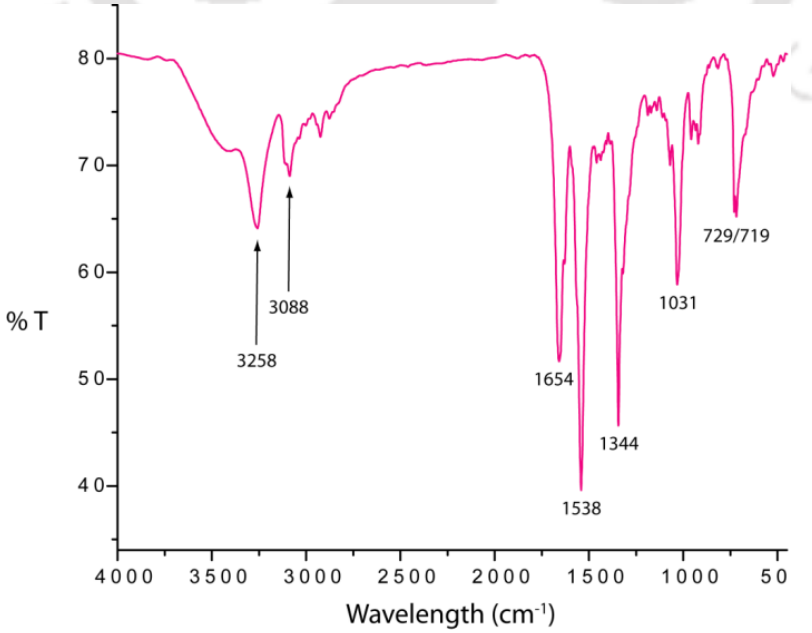

Figure A4.6 FT-IR spectrum of solvate **3a-IV** recorded in KBr pellet.

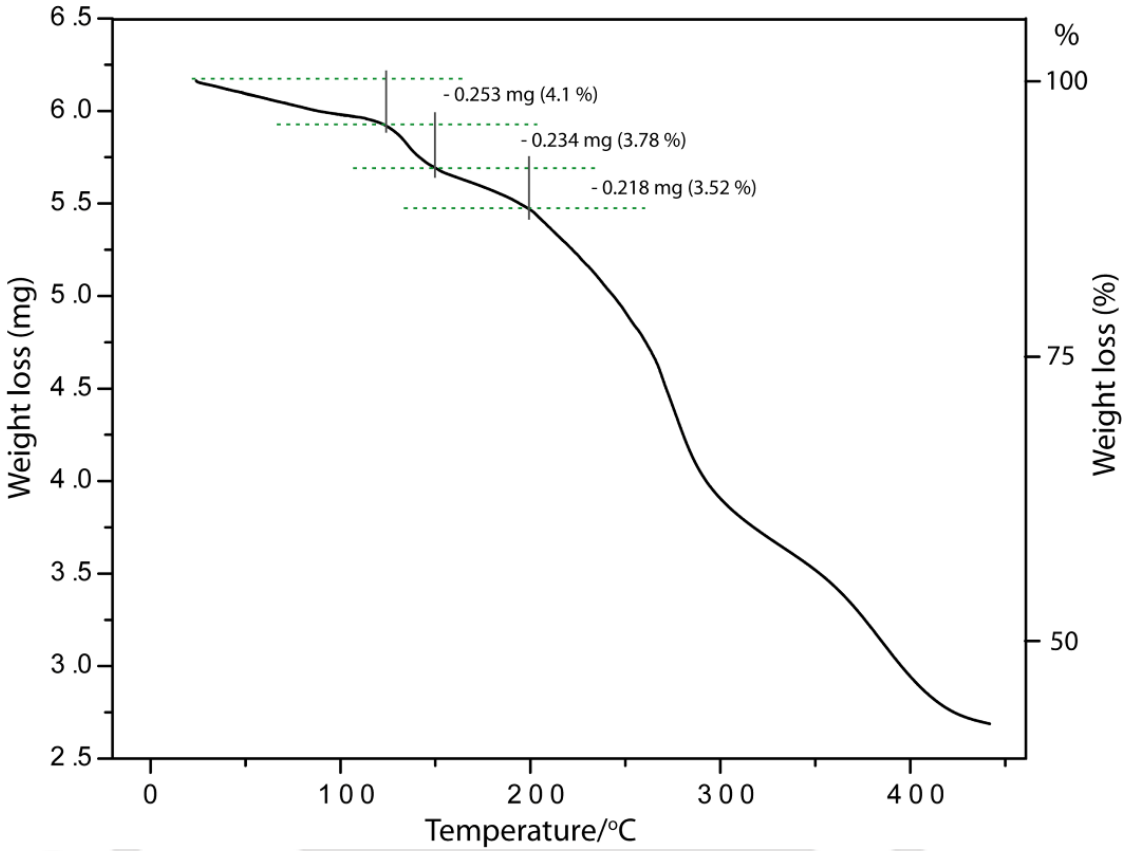

Figure A4.7 Thermo gravimetric curve of complex TBA[**L**(F)]•3THF (**3a-III**) at a heating rate of 10 °C/min in a N_2 atmosphere.

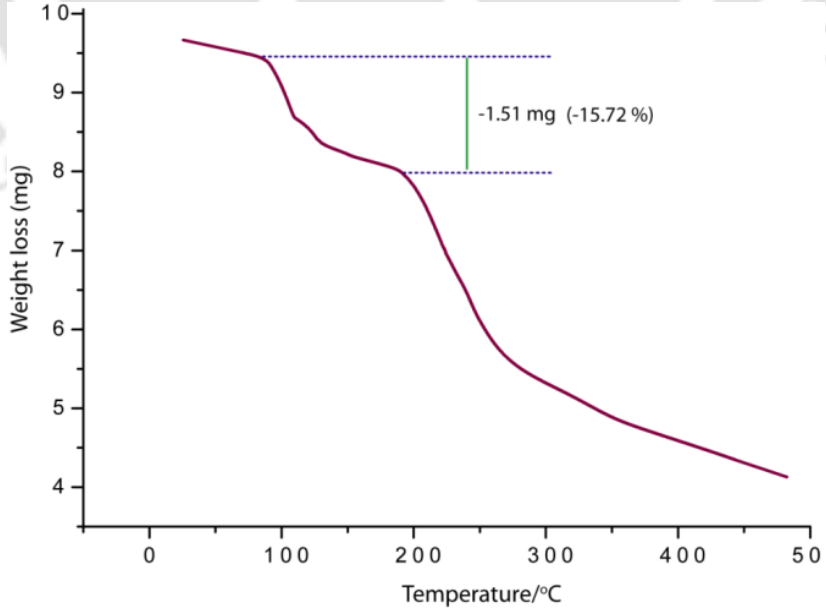

Figure A4.8 Thermo gravimetric curve of complex TBA[**L**(F)]•2DMSO-4H_2O (**3a-IV**) at a heating rate of 5°C/min in a N_2 atmosphere.

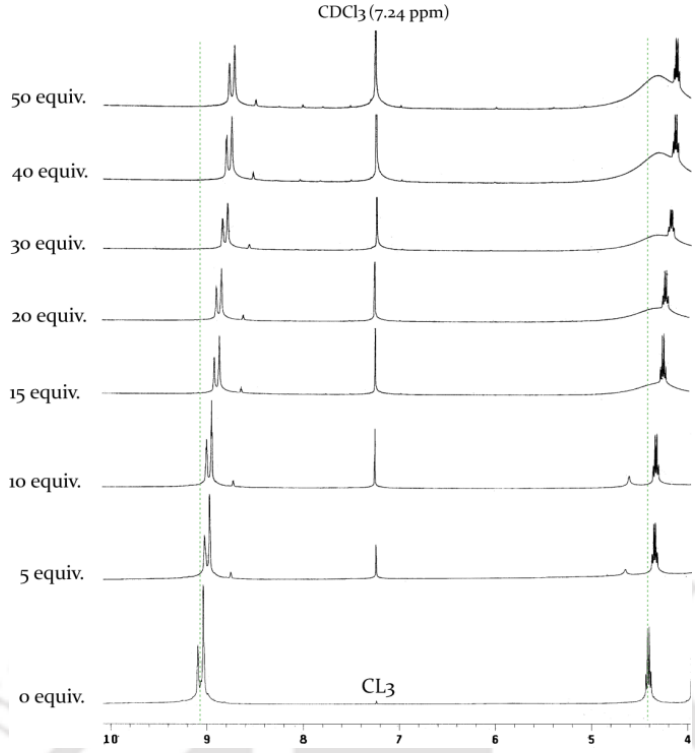

Figure A4.9 Partial ^{1}H NMR spectra showing the titration of **CL$_3$** ($CDCl_3$) upon increasing equivalents of TBAF.

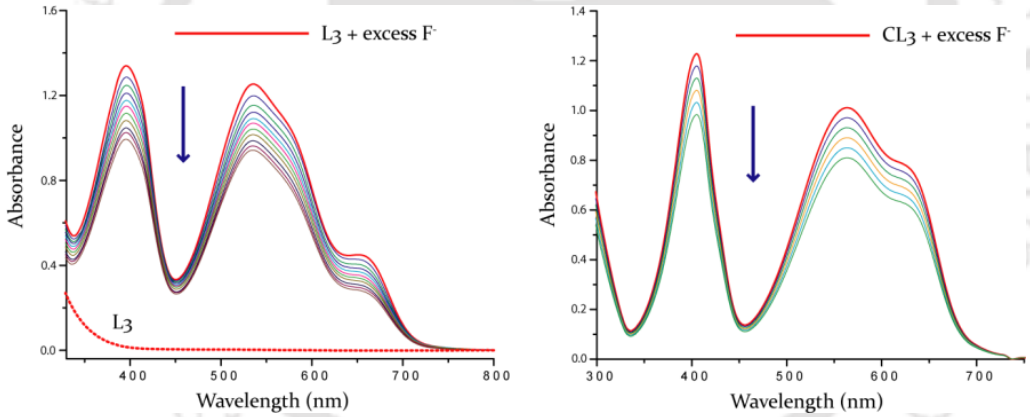

Figure A4.10 UV-Vis titration curves of **L$_3$** (left) and **CL$_3$** (right) charged with excess F^- in dry DMSO upon gradual addition of water (up to 1 mL).

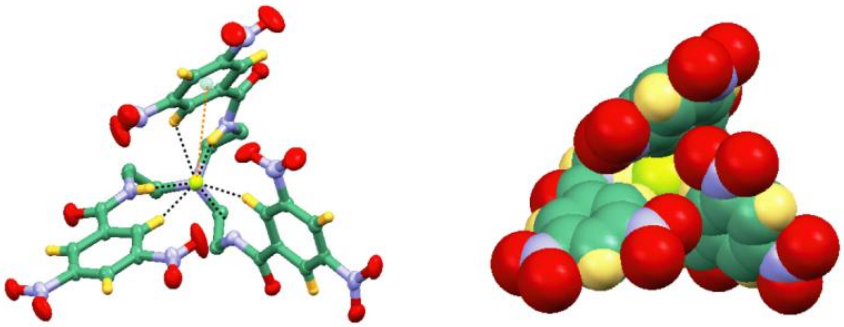

Figure A4.11 X-ray structure (thermal ellipsoid plot with 30% probability and space fill model) of F^-–encapsulated complex TBA[**L$_3$**(F)]2DMSO•4H_2O (**3a-IV**) showing binding and encapsulation of F^- within the receptor cavity. TBA cation and solvent molecule(s) are omitted for clarity in each case.

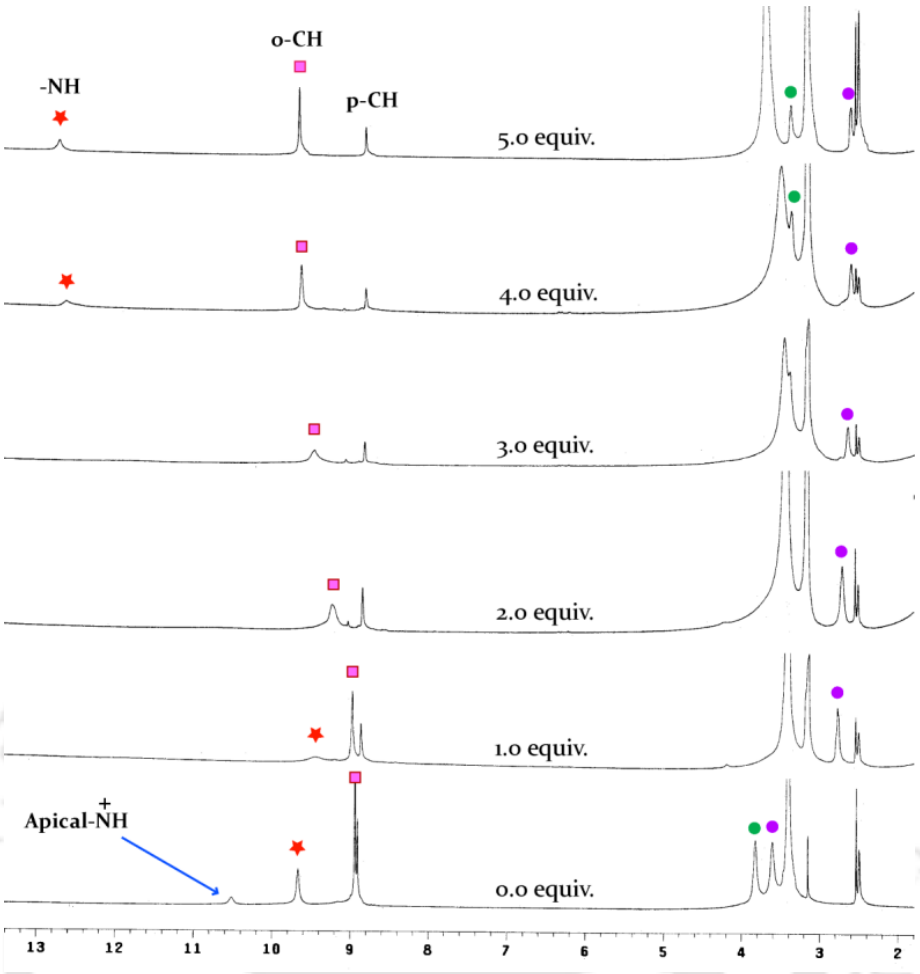

Figure A4.12 Partial ^{1}H NMR spectra showing the titration of complex **3c** ($CDCl_3$) with increasing equivalents of TBAF.

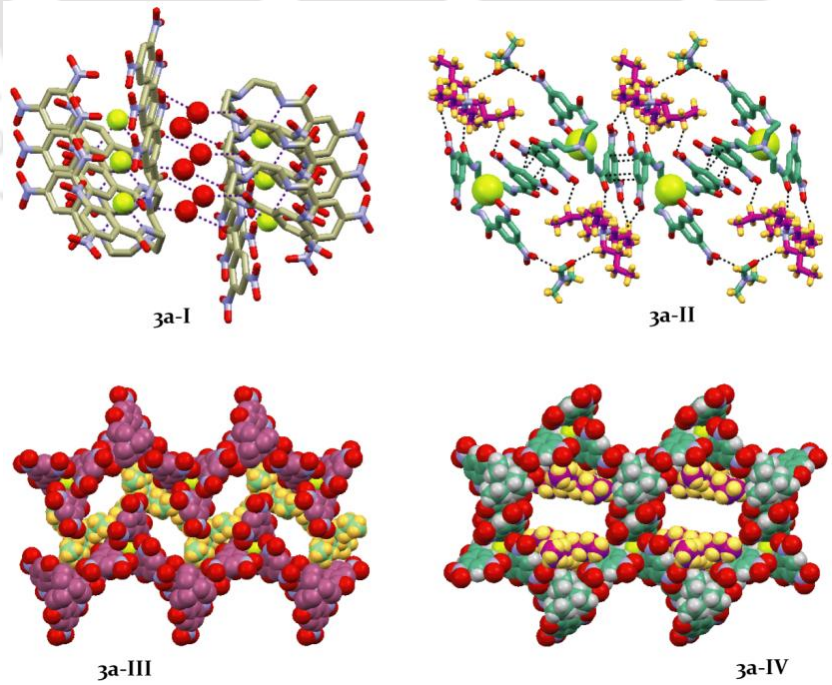

Figure A4.13 Crystal packing motifs of solvatomorphs of F^-–encapsulated complex, **3a I-IV**.

Annexure 5

Table A5.1 Hydrogen bonding interactions involved in the crystal structure of $\mathbf{L_4}$.

D-H····O	*d*(H····O)/Å	*d*(D····O)/Å	<D-H····O/^{o}
N2-H····O7	2.15(2)	2.948(3)	154(1)
N3-H····O7	2.04(1)	2.850(2)	156(1)
N12-H····O16	2.18(2)	2.973(3)	151(1)
N13-H····O16	2.00(1)	2.822(2)	159(1)
N5-H····O1	2.35(2)	3.018(3)	138(1)
N6-H····O1	2.10(2)	2.910(3)	156(1)
N8-H····O4	2.15(1)	2.942(2)	152(1)
N9-H····O4	2.14(1)	2.943(2)	154(1)
N15-H····O10	2.28(2)	2.974(2)	137(1)
N16-H····O10	2.04(1)	2.862(2)	159(1)
N18-H····O13	2.16(1)	2.961(2)	154(1)
N19-H····O13	2.23(1)	3.030(2)	153(1)
C1-H(A)····O12	2.71(2)	3.631(3)	157(1)
C20-H(A)····O12	2.66(2)	3.491(3)	143(1)
C35-H····O3	2.57(3)	3.338(4)	139(2)
C53-H····O9	2.66(2)	3.388(3)	135(2)
C34-H····C1g	3.21	4.027	147

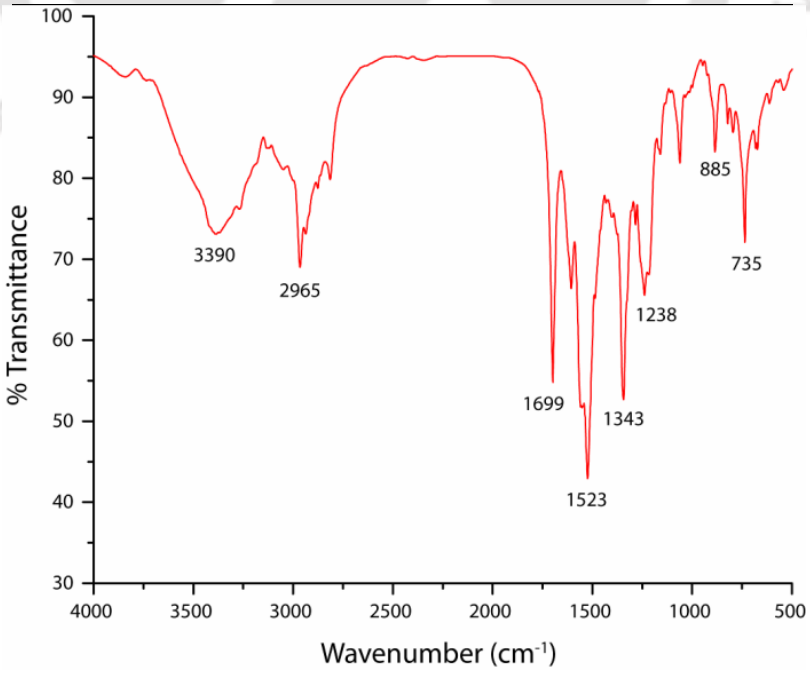

Figure A.5.1 FT-IR spectrum of complex **4a** recorded in KBr pellet.

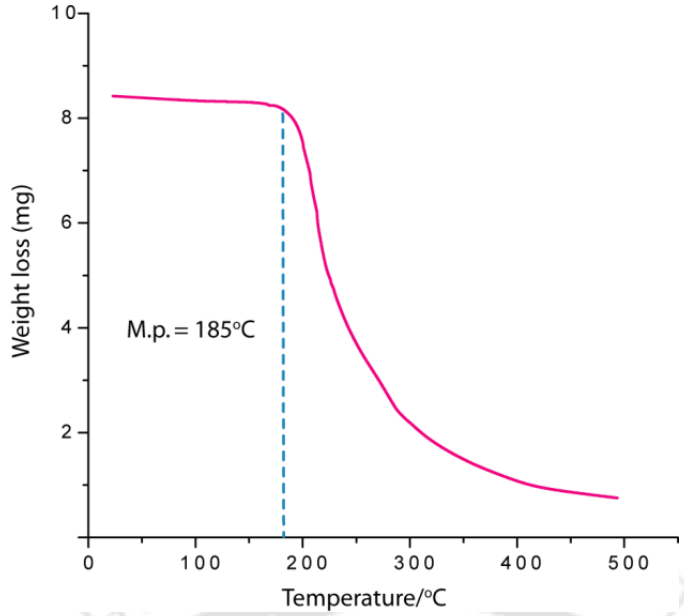

Figure A5.2 Thermo gravimetric (TGA) curve of complex **4a** obtained at a heating rate of 5°C/min in N_2 atmosphere.

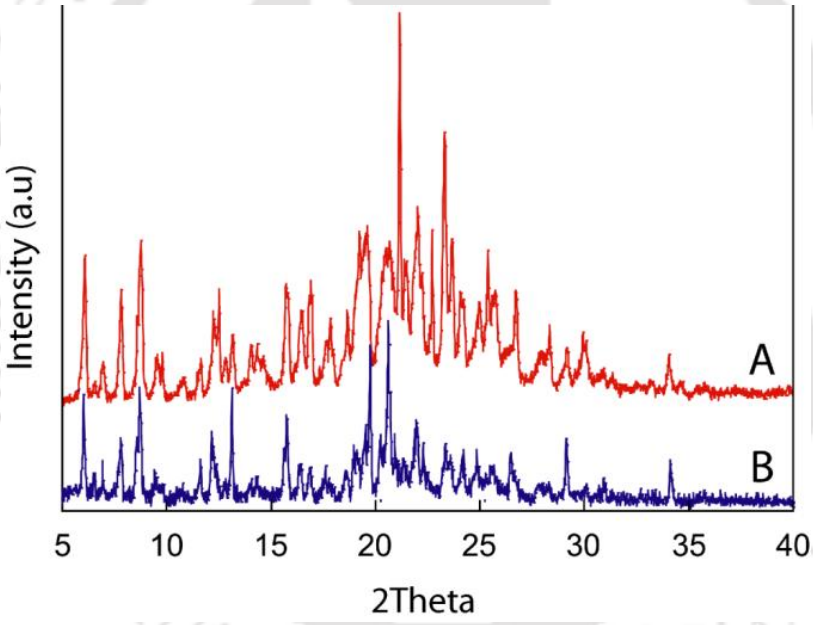

Figure A5.3 Powder X-ray diffraction patterns of isolated crystals of **4a** from (A) the receptor-OH^- solution and (B) receptor-F^- solution.

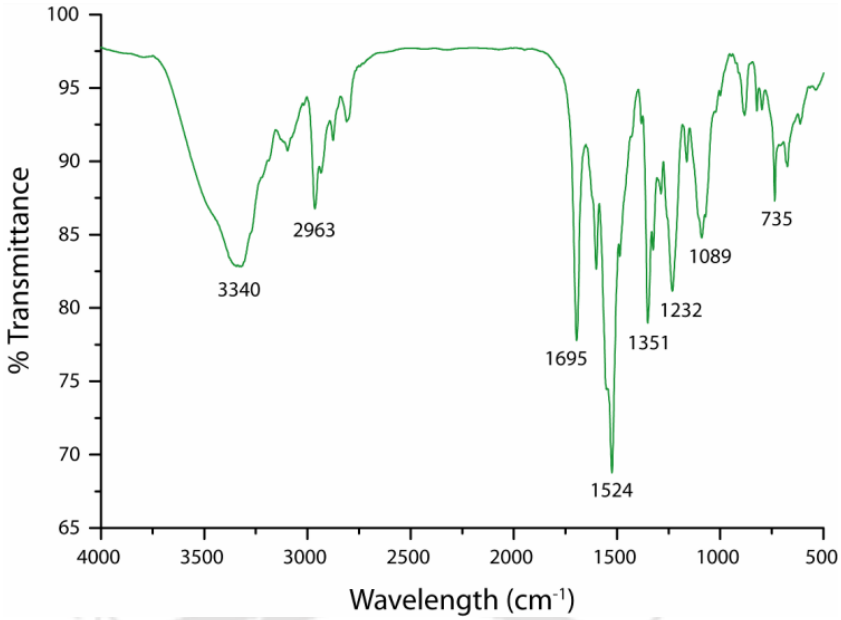

Figure A.5.4 FT-IR spectrum of complex **4b** recorded in KBr pellet.

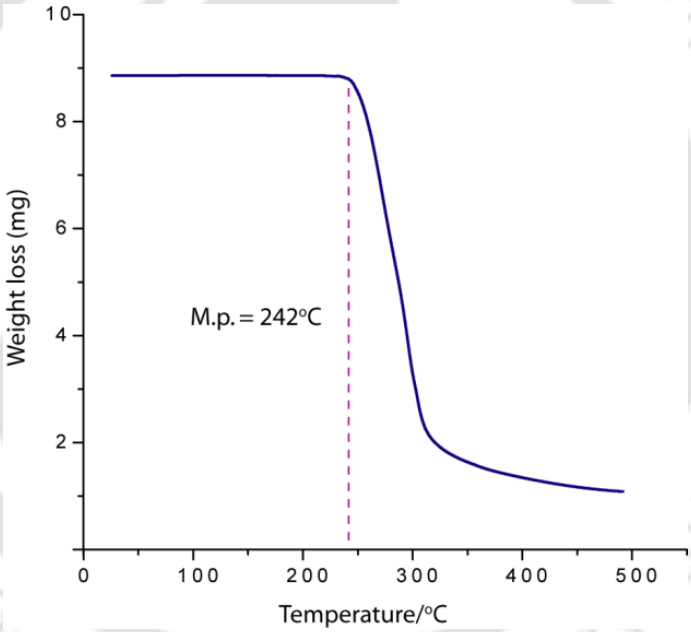

Figure A5.5 Thermo gravimetric (TGA) curve of complex **4b** obtained at a heating rate of 5°C/min in N_2 atmosphere.

Annexure 6

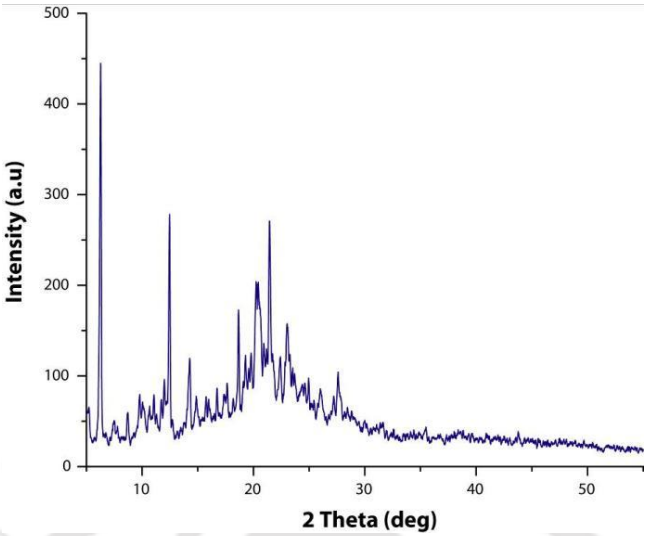

Figure A6.1 Powder XRD patterns of complex **5b-I** recorded with dried crystalline powders.

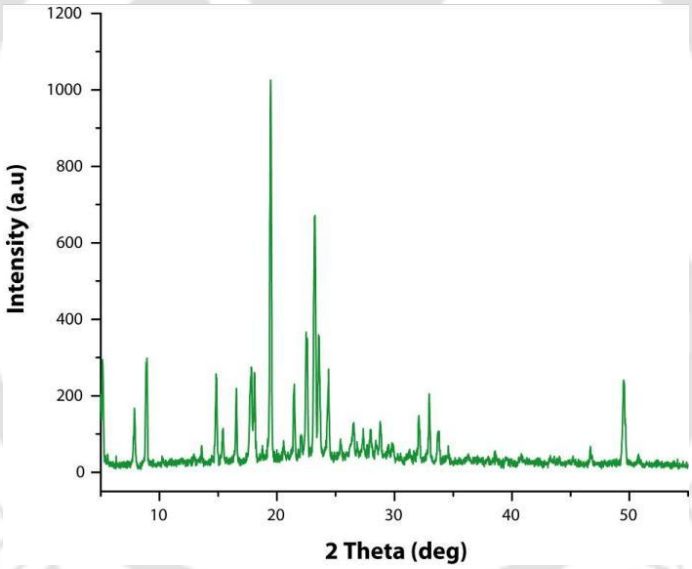

Figure A6.2 Powder XRD patterns of complex **5b-II** recorded with dried crystalline powders.

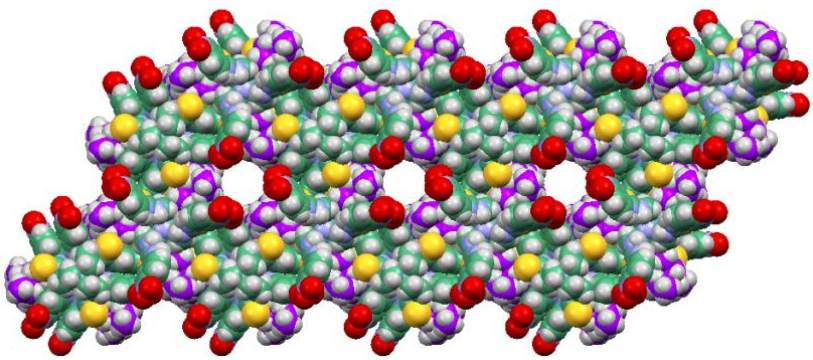

Figure A6.3 Crystal packing diagram of complex **5b-II**, showing the cylindrical voids of 568 $Å^3$ (view down the crystallographic c-axis).

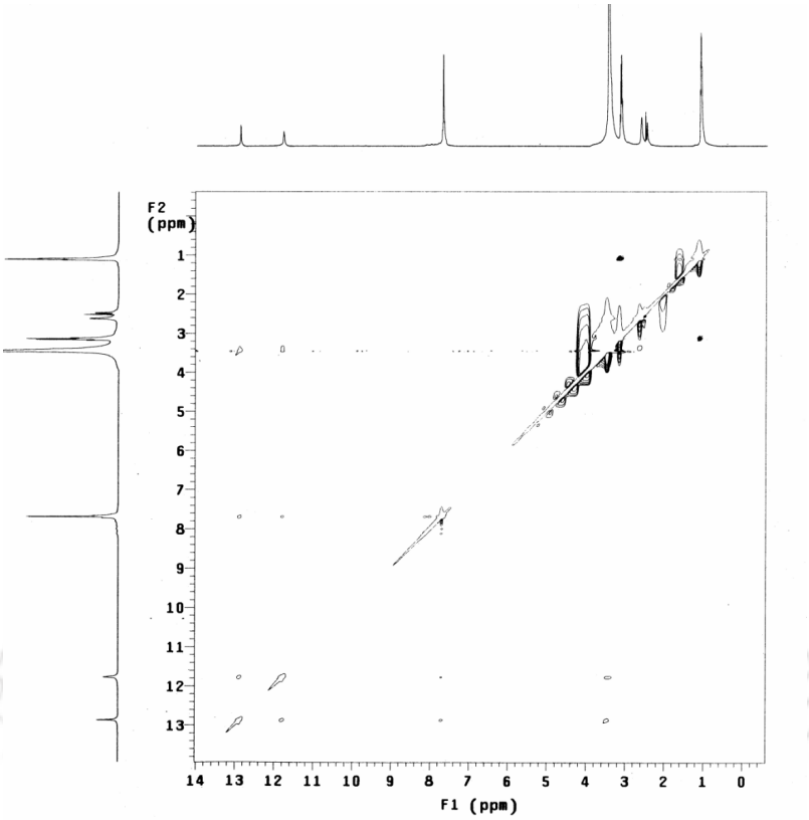

Figure A6.4 2D-NOESY NMR spectrum of complex **5b-II** in DMSO-d_6.

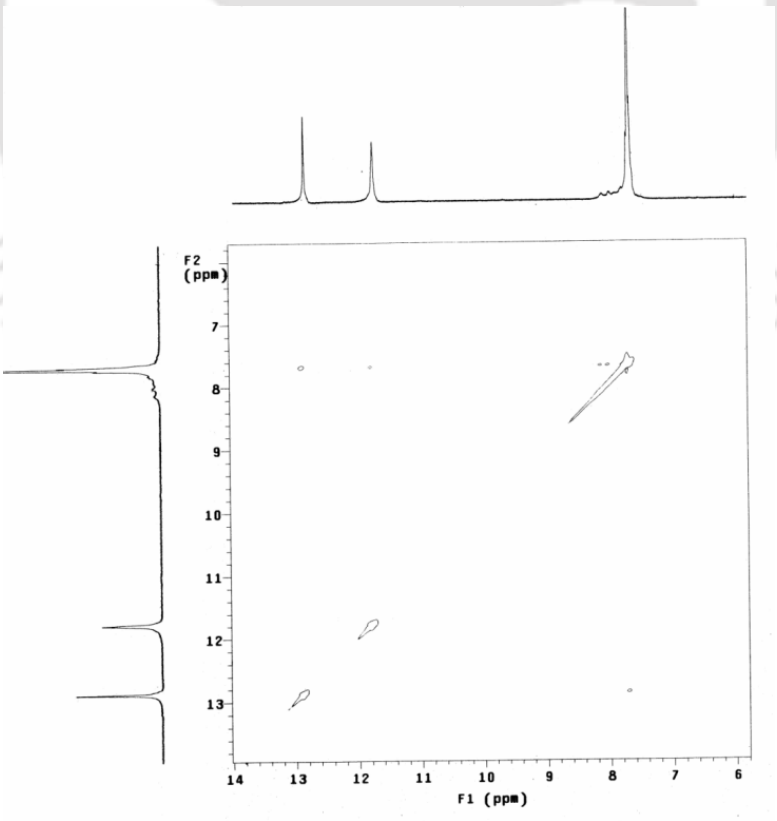

Figure A6.5 Partial (aromatic region) 2D-NOESY NMR spectrum of complex **5b-II** in DMSO-d_6, in presence of 0.5 equivalent 2:1 mixture of TBA(OH) and TBA(H_2PO_4).

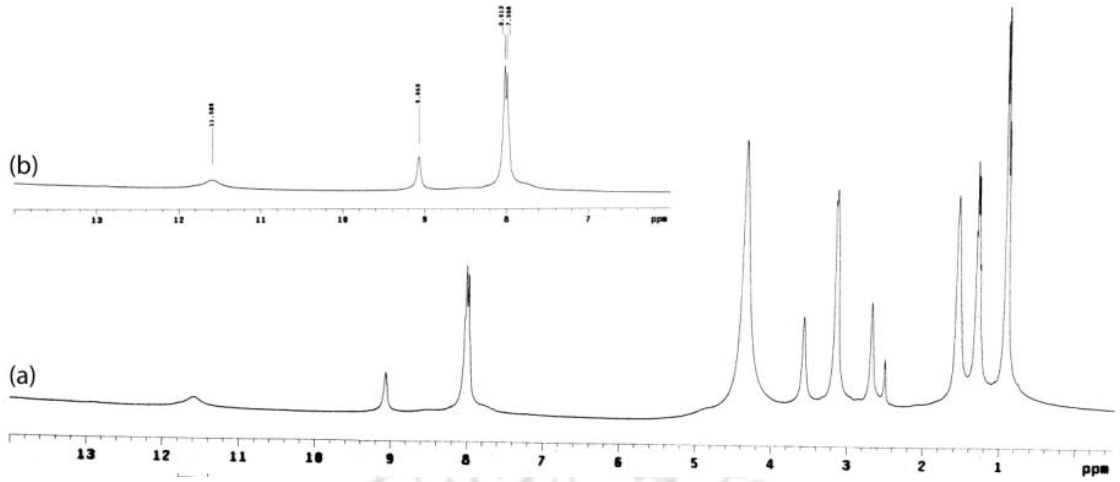

Figure A6.6 (a) ^{1}H NMR spectrum of $\mathbf{L_5}$ in presence of 1 equivalent of $TBAH_2PO_4^-$ recorded after overnight equilibration in DMSO-d_6; (b) Partial ^{1}H NMR spectrum (aromatic region), suggesting that PO_4^{3-}encapsulated complex does not form at equivalent stoichiometry of $H_2PO_4^-$.

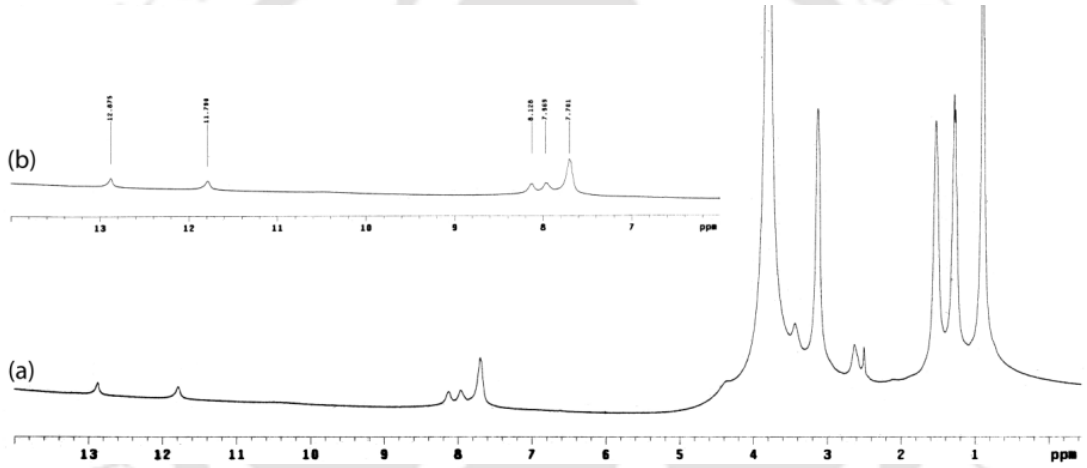

Figure A6.7 (a) ^{1}H NMR spectrum of $\mathbf{L_5}$ in presence of 3 equivalent of $TBAH_2PO_4^-$ recorded after overnight equilibration in DMSO-d_6; (b) Partial ^{1}H NMR spectrum (aromatic region), suggesting the in situ formation of PO_4^{3-}encapsulated complex in a comparatively greater percentage than the complex formed between added $H_2PO_4^-$ and $\mathbf{L_5}$.

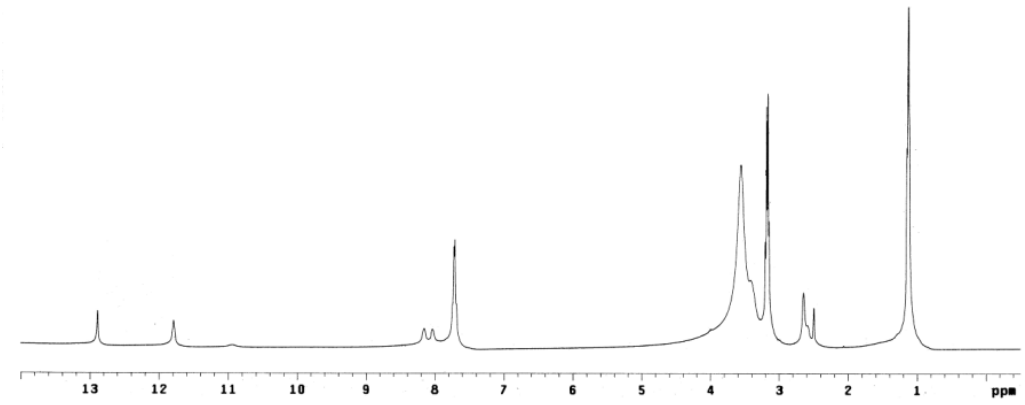

Figure A6.8 ^{1}H NMR spectrum of complex **5a** in presence of excess TEA(AcO) in DMSO-d_6 showing the selective formation of phosphate-encapsulated complex in solution.

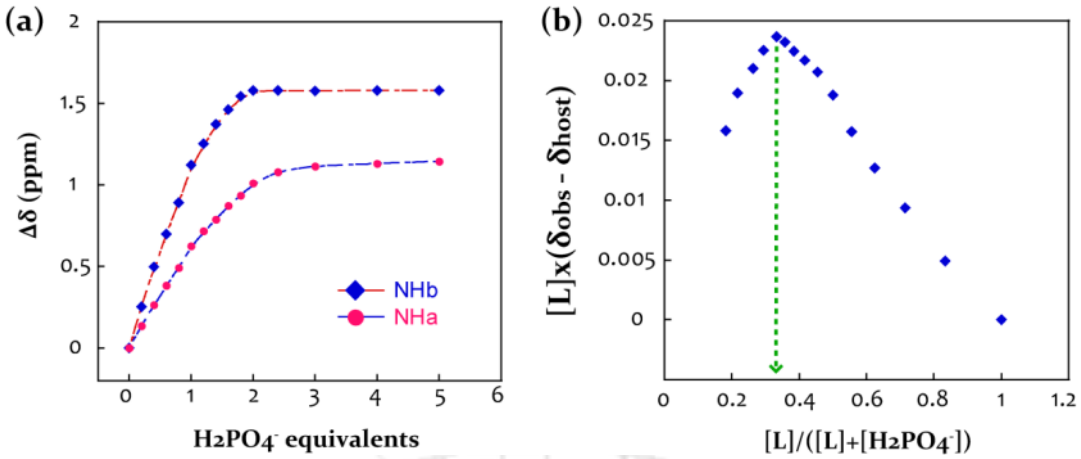

Figure A6.9 (a) Change in chemical shift of –NH resonances of $\mathbf{L_5}$ (10 mM) with increasing conc. of standard $H_2PO_4^-$ solution (50 mM) in DMSO-d_6; (b) The Job's plot.

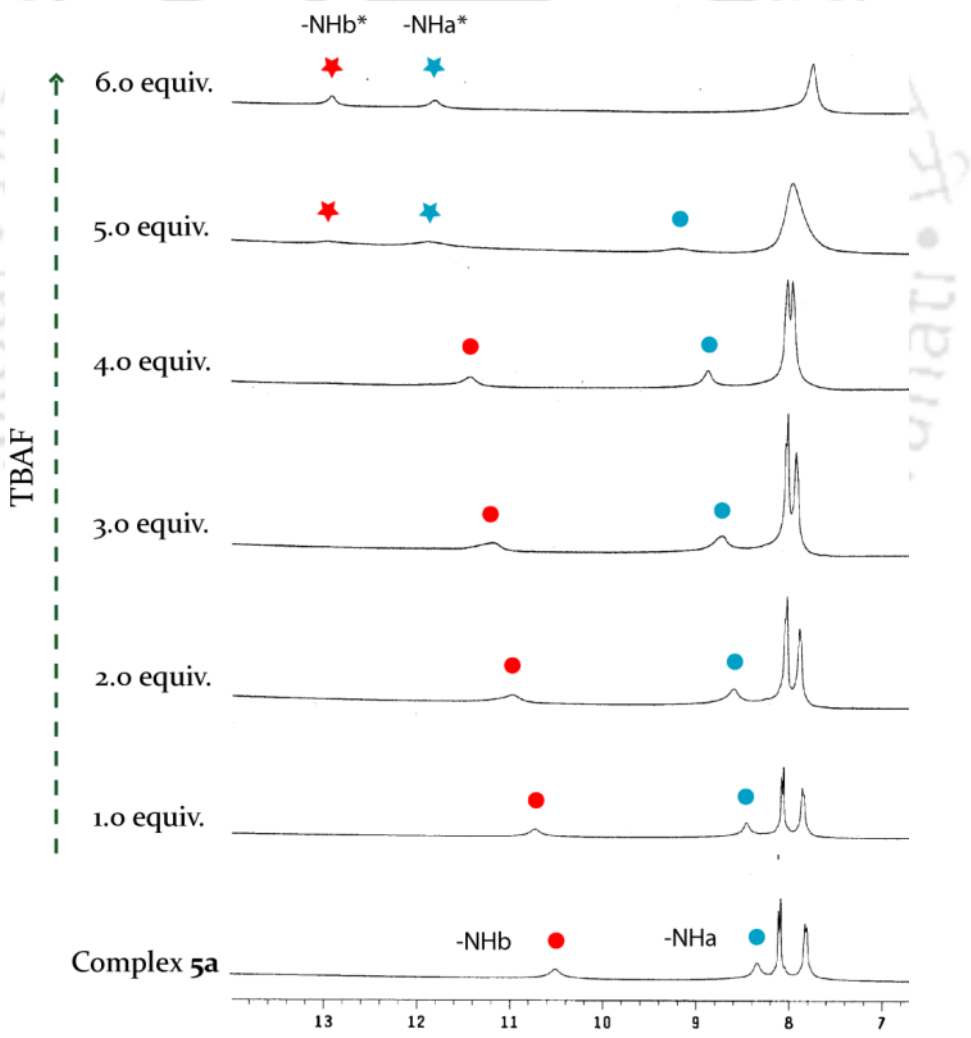

Figure A6.10 Partial ^{1}H NMR titration spectra of complex **5a** (10 mM) recorded with increasing equivalents of TBAF salt.